

# The Liver Tumor Segmentation Benchmark (LiTS)

Patrick Bilic<sup>1a</sup>, Patrick Ferdinand Christ<sup>1a</sup>, Eugene Vorontsov<sup>1e,1</sup>, Grzegorz Chlebus<sup>r</sup>, Hao Chen<sup>m,1</sup>, Qi Dou<sup>m</sup>, Chi-Wing Fu<sup>m</sup>, Xiao Han<sup>p</sup>, Pheng-Ann Heng<sup>m</sup>, Jrgen Hesser<sup>q</sup>, Samuel Kadoury<sup>e,1</sup>, Tomasz Kopczyski<sup>v</sup>, Miao Le<sup>o</sup>, Chunming Li<sup>o</sup>, Xiaomeng Li<sup>m</sup>, Jana Lipková<sup>a</sup>, John Lowengrub<sup>n</sup>, Hans Meine<sup>r</sup>, Jan Hendrik Moltz<sup>r</sup>, Chris Pal<sup>e,1</sup>, Marie Piraud<sup>a</sup>, Xiaojuan Qi<sup>m</sup>, Jin Qi<sup>l,1</sup>, Markus Rempfler<sup>a</sup>, Karsten Roth<sup>q</sup>, Andrea Schenk<sup>r</sup>, Anjany Sekuboyina<sup>a</sup>, Ping Zhou<sup>k</sup>, Christian Hülsemeyer<sup>a</sup>, Marcel Beetz<sup>a</sup>, Florian Ettlinger<sup>a</sup>, Felix Gruen<sup>a</sup>, Georgios Kaassis<sup>b</sup>, Fabian Lohfer<sup>b</sup>, Rickmer Braren<sup>b</sup>, Julian Holch<sup>c</sup>, Felix Hofmann<sup>c</sup>, Wieland Sommer<sup>c</sup>, Volker Heinemann<sup>c</sup>, Colin Jacobs<sup>d</sup>, Gabriel Efrain Humpire Mamani<sup>d</sup>, Bram van Ginneken<sup>d</sup>, Gabriel Chartrand<sup>e</sup>, An Tang<sup>e</sup>, Michal Drozdza<sup>e</sup>, Samuel Kadoury<sup>e</sup>, Avi Ben-Cohen<sup>f</sup>, Eyal Klang<sup>f</sup>, Marianne M. Amitai<sup>f</sup>, Eli Konen<sup>f</sup>, Hayit Greenspan<sup>f</sup>, Johan Moreau<sup>g</sup>, Alexandre Hostettler<sup>g</sup>, Luc Soler<sup>g</sup>, Refael Vivanti<sup>h</sup>, Adi Szeskin<sup>h</sup>, Naama Lev-Cohain<sup>h</sup>, Jacob Sosna<sup>h</sup>, Leo Joskowicz<sup>h</sup>, Ashnil Kumar<sup>w</sup>, Avinash Kore<sup>x</sup>, Chunliang Wang<sup>y</sup>, Dagan Feng<sup>z</sup>, Fan Li<sup>aa</sup>, Ganapathy Krishnamurthi<sup>x</sup>, Jian He<sup>ab</sup>, Jianrong Wu<sup>aa</sup>, Jinman Kim<sup>x</sup>, Jinyi Zhou<sup>ac</sup>, Jun Ma<sup>ad</sup>, Junbo Li<sup>aa</sup>, Kevis-Kokitsi Maninis<sup>ae</sup>, Krishna Chaitanya Kaluva<sup>x</sup>, Lei Bi<sup>x</sup>, Mahendra Khened<sup>x</sup>, Miriam Beliver<sup>ae</sup>, Qizhong Lin<sup>aa</sup>, Xiaoping Yang<sup>ad</sup>, Yading Yuan<sup>af</sup>, Yinan Chen<sup>aa</sup>, Yuanqiang Li<sup>ad</sup>, Yudong Qiu<sup>s</sup>, Yuli Wu<sup>ad</sup>, Bjoern Menze<sup>a</sup>

<sup>a</sup>Department of Informatics, Technical University of Munich, Germany

<sup>b</sup>Institute of Radiology, Technical University of Munich, Germany

<sup>c</sup>Ludwig Maximilian University of Munich, Department of Clinical Radiology

<sup>d</sup>Radboud University Medical Center, Nijmegen, Netherlands

<sup>e</sup>École Polytechnique de Montréal, Montréal, Canada

<sup>f</sup>Centre de recherche du CHUM, Montreal, Canada

<sup>g</sup>Tel Aviv University and Sheba Medical Center, Tel Aviv, Israel

<sup>h</sup>IRCAD Institute, Strasbourg, France

<sup>i</sup>The Hebrew University of Jerusalem and Hadassah University Medical Center, Jerusalem, Israel

<sup>j</sup>Montreal Institute for Learning Algorithms (MILA), Montreal, Canada

<sup>k</sup>Cancer/Hospital Center, University of Electronic Science and Technology of China, Chengdu, China

<sup>l</sup>Center for Information in Medicine, University of Electronic Science and Technology of China, Chengdu, China

<sup>m</sup>Department of Computer Science and Engineering, The Chinese University of Hong Kong

<sup>n</sup>Departments of Mathematics, Biomedical Engineering, Chemical Engineering and Materials Science & Center for complex Biological Systems & Chao Family Comprehensive Cancer Center, University of California, Irvine, USA

<sup>o</sup>Electrical Engineering Department, University of Electronic Science and Technology of China, Chengdu, China

<sup>p</sup>Elekta, Inc, St. Louis, USA

<sup>q</sup>Experimental Radiation Oncology, Department of Radiation Oncology, University Medical Center Mannheim, Heidelberg University, Germany

<sup>r</sup>Fraunhofer Institute for Medical Image Computing MEVIS, Bremen, Germany

<sup>s</sup>Insight Medical Technology, Inc

<sup>t</sup>Medical Image Computing Group, University of Bremen, Bremen, Germany

---

<sup>1</sup>Authors contributed equally

<sup>u</sup>*Montreal Institute for Learning Algorithms (MILA), Montreal, Canada*

<sup>v</sup>*Volume Graphics GmbH, Heidelberg, Germany*

<sup>w</sup>*School of Computer Science, The University of Sydney, Australia*

<sup>x</sup>*Department of Engineering Design, Indian Institute of Technology Madras, India*

<sup>y</sup>*Department of Medical Image Processing and Visualization, KTH Royal Institute of Technology, Sweden*

<sup>z</sup>*School of Information Technologies, The University of Sydney, Australia*

<sup>aa</sup>*Philips Research China, China*

<sup>ab</sup>*Department of Radiology, Nanjing Drum Tower Hospital, China*

<sup>ac</sup>*Department of Chemistry, Tianjin University, China*

<sup>ad</sup>*Department of Mathematics, Nanjing University of Science and Technology, China*

<sup>ae</sup>*Computer Vision Lab, ETH Zurich, Switzerland*

<sup>af</sup>*Icahn School of Medicine at Mount Sinai, USA*

<sup>ag</sup>*Department of Hepatopancreatobiliary Surgery, Nanjing Drum Tower Hospital, China*

---

## Abstract

In this work, we report the set-up and results of the Liver Tumor Segmentation Benchmark (LiTS) organized in conjunction with the IEEE International Symposium on Biomedical Imaging (ISBI) 2017 and International Conference On Medical Image Computing & Computer Assisted Intervention (MICCAI) 2017. Twenty-four valid state-of-the-art liver and liver tumor segmentation algorithms were applied to a set of 131 computed tomography (CT) volumes with different types of tumor contrast levels (hyper-/hypo-intense), abnormalities in tissues (metastasectomy) size and varying amount of lesions. The submitted algorithms have been tested on 70 undisclosed volumes. The dataset is created in collaboration with seven hospitals and research institutions and manually blind reviewed by independent three radiologists. We found that not a single algorithm performed best for liver and tumors. The best liver segmentation algorithm achieved a Dice score of 0.96(MICCAI) whereas for tumor segmentation the best algorithm evaluated at 0.67(ISBI) and 0.70(MICCAI). The LiTS image data and manual annotations continue to be publicly available through an online evaluation system as an ongoing benchmarking resource.

*Keywords:* Liver; Tumor; CT; Segmentation; Medical imaging, Benchmark.

---

## 1. Introduction

Due to its detoxification function the liver one of the essential organs in the human body. Radiologists and oncologists analyze computed tomography (CT) or magnetic resonance images (MRI) to study livers' anomalies in shape and texture. These anomalies are important biomarkers for initial disease diagnosis and progression in both primary and secondary hepatic tumor disease [1, 2]. Often primary tumors of the abdomen such as breast, colon and pancreas cancer spread metastases to the liver during the course of disease. Therefore, the liver and its lesions are routinely analyzed in primary tumor staging. The RECIST protocol, which states to measure the diameter of the largest target lesion, has become clinical reference standard in tumor staging of liver cancer[3]. From a global perspective primary liver cancer is the second most common cause of cancer death and is the sixth most frequent cancer [4]. Computed tomography (CT) is the most commonly used image modality by radiologists and oncologists for liver lesion evaluation and staging[5]. Furthermore, segmenting malignant liver tissues is important for cancer diagnosis, treatment, planning, and tracking treatment response. In addition, liver and tumor segmentation is also a prerequisite or a key asset for many treatment options such as thermal percutaneous ablation[6], percutaneous ethanol injection[7], radiotherapy surgical resection[8] and arterial embolization[9]. However diagnostic imagery is expensive, very time-consuming, poorly reproducible and its segmentations show operator-dependent results.

Since tumor volume is a better predictor than diameter, according to the Response Evaluation Criteria in Solid Tumor (RECIST), automatic segmentation is the most desirable goal [10, 11].

However, a fully-automated segmentation of liver and its lesion remains still an open problem because different acquisition protocols, differing contrast-agents, varying levels of contrast enhancements and dissimilar scanner resolutions lead to unpredictable intensity differences between liver and lesion tissue [12]. Many different types of lesions and especially tumor sub-types can occur in affected livers. Thus, these different types of tumors with varying contrast levels (hyper-/hypo-intense tumors) form obstacles to overcome. Modern methods struggle with abnormalities in tissues (such as after surgical resection of metastasis) or the size, shape and varying number of lesions [12].

Over the last 30 years computational liver and liver tumor segmentation has attract considerable attention, by a wide range of methods for automated, semi-automated and interactive segmentation [12]. All of these methods were validated on either relatively small datasets, private data sets or the segmentations are available either for liver or liver tumors.

Therefore, it remains difficult to judge which methods will worthwhile to pursue in research and clinical practice. Furthermore, the exact performance of the best algorithms available today can not be can not be determined unequivocally. Moreover, and how well current segmentations generated by automated computational methods compare with human expert groups ratings.

In order to judge the current state-of-the-art in automated liver and liver tumor segmentation and compare different methods, we organized the Liver Tumor Segmentation Challenge (LiTS) in conjunction with the IEEE International Symposium on Biomedical Imaging

(ISBI) 2017 and with the conference on Medical Image Computing and Computer Assisted Interventions (MICCAI) 2017. Compared to ISBI 2017 we added tasks for liver segmentation and tumor burden estimation for MICCAI 2017. We prepared a unique dataset of 201 CT scans of patients with hepatocellular carcinoma (HCC) including expert ground-truth segmentations of liver and tumor lesions and made it publicly available. The dataset is created in collaboration with seven hospitals and research institutions and manually reviewed by independent three radiologists. As shown in figure 1 the heterogeneity in liver and lesion contrast is very large among subjects. The contrast, size and shape of liver lesions varies a lot among subjects as shown in figure 1 and in particular their corresponding histograms. This complexity of contrast differences make it difficult for intensity-based methods to generalize to unseen test cases from different clinical sites. In addition, the varying shape of lesions due to irregular tumor growth and response to treatment (i.e surgical resection) reduce efficiency of computational methods that make use of prior knowledge on lesion shape in particular shape-based methods, which have gained large attraction in organ segmentation.

The tumor burden, which is defined as the liver/tumor ratio plays an important role in surgical resection planning [13, 14]. Instead of measuring diameters of target lesions, a fully volumetric segmentation of both liver and its lesion and the subsequent tumor burden analysis offers valuable insights of the disease progression [15]. Further, tumor burden is also important in assessing the effectiveness of different treatment and can therefore potentially replace the RECIST protocol [16, 17, 18, 19, 20, 21]. A fully automatic liver and tumors segmentation allows easier computation of tumor burden and consequently simplifying the surgical liver resection planning.

Our contributions are three-fold. First a new reference dataset of 201 abdominal CT Volumes (131 training, 70 test) including liver and liver tumor ground truth segmentations is released. Second, the set-up and learnings of our medical image benchmark, which was presented as two Grand Challenges organized in conjunction with ISBI 2017 and MICCAI 2017 is described. Third, the resulting state-of-the-art algorithms of the benchmark are reviewed, evaluated and ranked.

The paper is structured as follows. We review the current state-of-the-art in automated liver segmentation and respectively liver tumor segmentation as well as relevant public datasets of liver and liver tumors, benchmark efforts in other biomedical image analysis tasks, in Section II. Following we describe the LiTS challenge set-up and its provided data set containing manual annotation of liver and tumor structures, and the evaluation process in Section III. Finally, we report and discuss the results of our comparisons in Section IV and V.. Section VI concludes the paper.

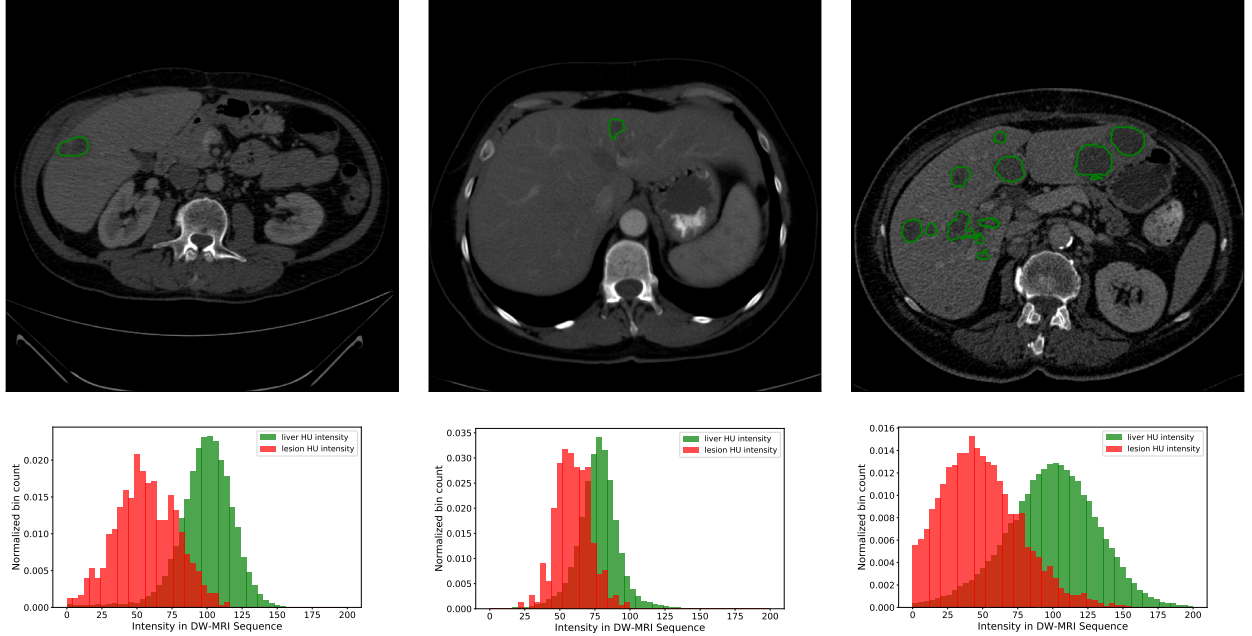


Figure 1: Excerpt of the benchmark dataset depicting the heterogeneity of abdominal CT scans and their corresponding HU-Level densities of liver and tumor areas.

## 2. Prior Work

The task of liver and liver tumor segmentation identifies a set of voxels which describes the region of liver in medical image. In the last decade the scientific work on liver and liver tumor segmentation has quadrupled (Fig. 2). Most of the available (semi-)automatic liver and tumor segmentation methods used traditional computer vision and machine learning methods. If machine learning based methods are used mostly multiclass classification of liver and tumor voxel/pixel are applied. The following section provides a grouped overview of published methods for (semi-) automated liver and liver tumor segmentation tasks.

### 2.1. Algorithms for Liver Segmentation

Published results of liver segmentation methods can be structured into four categories: methods based on *spatial and geometric prior knowledge*(1), *local image features with spatial context*(2) *local image features with voxel-wise classification*(3) and neural networks(4). Furthermore there are semi-automated solutions(5) utilizing methods mentioned above.

#### (1) Methods based on spatial and geometric prior knowledge

Over the last two decades statistical Shape Models (SSMs)[22] have been used for automatic liver segmentation task. However, deformation limitations prevent SSMs capturing of the high variability of the liver shapes. To overcome this problem SSMs approaches often rely on an additional step for obtaining a finer segmentation contour. Therefore SSMs followed by a deformable model performing free form deformation had become a valuable

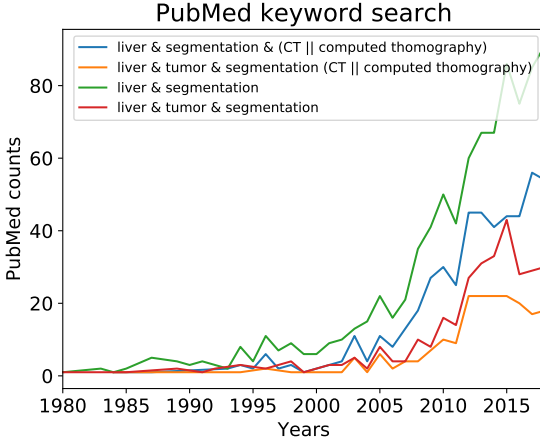


Figure 2: Results of PubMed searches for liver segmentation (green) and liver tumor segmentation (red) on CT images (blue and orange). In the 80s and 90s, the number of publications involving liver and liver tumor segmentation has seen nearly no increase. Starting from 2005 the number of publications have risen significantly.

method for liver segmentation[23, 24, 25, 26, 27, 28]. Moreover, variations and further enhancement of SSM such as 3D-SSM based on an intensity profiled appearance model [29], incorporating non-rigid template matching [30], initialization of SSMs utilizing an evolutionary algorithm [24], hierarchical SSMs [31], and deformable SSM [26] had been proposed to solve liver segmentation tasks automatically.

## (2) Methods based local image features and spacial context

A probabilistic atlas (PA) is a specific model for a population of images with parameters that are learned from a training dataset. Park et al. proposed the first PA utilizing 32 abdominal CT series for registration based on mutual information and thin plate splines as warping transformations[32] and a Markov random field (MRF)[32] for segmentation. Further proposed atlas based methods differ in their computation of PA and the way the PA is incorporated into the segmentation task. Furthermore, PA can incorporate relations between adjacent abdominal structures to define an anatomical structure surrounding the liver [33]. Multi-atlas improved atlas based liver segmentation results by using non-rigid registration with a B-spline transformation model[34], dynamic atlas selection and label fusion[35], liver and non-liver voxel classification based on k-Nearest Neighbors (kNN) [36]. Furthermore, Okada et al. proposed a method combining PA and SSM [37].

Gray level methods utilize statistics to estimate the intensity distribution of the liver. Lim et al. proposed several methods to segment liver using morphological filters and intensity distributions[38, 39], and pattern features[40]. Graph Cut (GC) methods segments the image into background and liver. All pixels respectively voxels of the image is represented by a set of vertices. Automatic methods describe graph cuts initialized by adaptive thresholding [41] supervoxel based graph cuts[42]. A combination of Graph Cut, SSM and PA is proposed by Shimizu et al [43]. Gao et al. proposed a rule based liver segmentation algorithm where

intensity and shape based rules are incorporated into the thresholding algorithm to include or exclude different regions of abdominal organs[44]. Other methods include fuzzy c-means based clustering[45], artificial bee colony clustering[46] in combination with morphological operations for segmentation refinement and random walk algorithms with automatic liver region detection for seed generation[47].

#### *(3) Methods based on local image features with voxel-wise classification*

Classification methods which solely concentrate on liver segmentation without tumors are rarely available. Existing, approaches combine AdaBoost classifier to identify location[48] or liver boundaries [49] and free-form deformation for segmentation refinement. Other feature based classification combine AdaBoost with random walk algorithms[50]. Multi-label liver and liver tumor classification methods are mentioned in 2.2.

#### *(4) Methods based on neural networks and deep learning*

The first proposed neural network used histogram features for liver segmentation in 1994. The approach heavily relied on pre- and post-processing to discard irrelevant regions upfront and ensure smooth boundaries by morphological operations and b-spline smoothing afterwards. [51] Modern convolutional Neural Networks is a data-driven algorithm which can be optimized end-to-end without hand-craft feature engineering. Today convolutional neural networks are widely used in automatic semantic segmentation tasks in medical imaging without reliance on hand-crafted features [52].

The U-Net architecture, introduced by Ronneberger et al., is widely used DCNN for biomedical image segmentation, and has already proven its efficiency and robustness in several segmentation tasks [53]. The architectural novelty in U-net over traditional semantic segmentation networks [54, 55] is the combination of an equal amount of upsampling and downsampling layers and the skip connections between its opposing convolution and deconvolution layers. Other approaches, similar to U-NET used 2D CNN, but without cross-connections overcame the challenge of low contrast between the liver and adjacent organs showed good results on SLIVER07 [56].

Successful methods share the commonality of multi-stage processes, beginning with a 3D CNN and use its learned probability maps as input for further post processing. We have seen good results on SLIVER07 both combining a simultaneous liver detection and probabilistic segmentation using 3D CNN with accuracy refinement of the segmentation afterwards using graph cut[57], 3D CNN in combination with random fields [58], 3D CNN following a surface evolution algorithm[59]. Moreover, a 3D CNN is has been proposed to learn a subject-specific probability map of the liver. Afterwards global and local appearance information is incorporated into a segmentation model which is globally optimized for surface evolution [59].

#### *(5) Semi-automated methods*

Automated segmentation methods require a large dataset for modeling the different variation of livers. Semi-automatic methods were generally regarded as more robust especially

in the case of irregular livers. However, segmentation results of semi-automatic methods are reliant on the operator skill and can differ. Semi-automated methods differ in their required degree of manual input. Popular methods such as region growing generally require often costly pre- and post processing in form of manual seed region initialization and segmentation refinement. However, advanced region growing methods show competitive results in 2D liver segmentation[60, 61] and 3D liver segmentation [62]. Graph cut (GC) segmentation [63] methods are in consequence of its semi-automatic ability to edit segmentation results interactively, suitable for clinical applications. A higher degree of costly user interaction using GC provides the potential to refine the liver segmentation [64]. Further, 2D to 3D interpolation methods based on shape models to reconstruct the whole 3D surface based on selected 2D contours [65, 66], and slice based segmentation using distance transformations of manual segmented upper and lower axial slices[67] are proposed. Other 3D segmentation approaches include a combination of k-means clustering and region growing followed by a contouring algorithm for refined segmentation based on a manually selected single slice [68] and active contour based segmentation using surface information provided by a level set method using a single manual seed inside the liver [69].

## 2.2. Algorithms for Liver Tumor Segmentation

Compared to liver tumor appearances differ in shape, size and contrast. In comparison to segment only one region of interest, liver tumors can materialize in different numbers of occurrences often with no clearly visible edges. Often contrast agents introduce additional noise in images. Therefore liver tumor segmentation is considered to be the more challenging task. Published methods of liver tumor segmentation can be categorized into *Thresholding methods*(1), *Spatial regularization methods*(2), *Local image features with supervised classification and unsupervised clustering methods*(3), *Deep Learning methods*(4). Furthermore there are *semi-automated* solutions (5) utilizing methods mentioned above.

### (1) Thresholding methods

Based on the assumption that gray levels of tumor areas differ from pixels belonging to regions outside the tumor, thresholding is a simple but effective tool to automatically separate tumor from liver and background shown first by Soler et al. 2001[70]. Since then thresholding based methods have set an adequate threshold value by histogram analysis[71], maximizing variance between classes[72] and iterative setting the threshold value by an isodata algorithm[73] to improve tumor segmentation results.

### (2) Spatial regularization methods

Spatial regulation techniques rely on (prior) information about the image or morphologies e.g. size, shape, surface or spatial information of tumors. This knowledge is used to introduce constraints in form of regularization or penalization. Adaptive thresholding methods can be combined with model-based morphological processing for heterogeneous lesion segmentation [74, 75]. Active contour[76] based tumor segmentation relies on shape and surface information and utilize probabilistic models[77] or histogram analysis[78] to create segmentation maps automatically. Level set[79] methods allow numerical computations of

tumor shapes without parametrization. Level set approaches for liver tumor segmentation are combined with supervised pixel classification in 2D[80] and 3D[81]. Furthermore, one proposed level set method is parametrized by probability vectors provided by an initial 2D CNN[82].

#### *(3) Local image features with supervised classification and unsupervised clustering methods*

Due to the heterogeneous occurrence of liver tumors machine learning based methods are well established in automatic liver tumor segmentation tasks. Clustering methods include k-means [83] and fuzzy c-means clustering with segmentation refinement using deformable models[84]. Among supervised classification methods are, a fuzzy classification based level set approach[80], Support Vector Machines (SVM) in combination with a texture based deformable surface model for segmentation refinement[85], AdaBoost trained on texture features[86] and image intensity profiles[87], logistic regression[88] and Random Forests (RF) recursively classifying and decomposing supervoxels[89].

#### *(4) Deep Learning methods*

Before LiTS, deep learning methods have been rarely used for liver tumor segmentation tasks. One approach introduced a 11-layer 3D CNN and graph cut for segmentation refinement[90] and Christ et al. proposed a dense 3D conditional random field for segmentation refinement after cascading 3D CNNs (U-Net) for liver and tumor segmentation [2].

#### *(5) Semi-automated methods*

Liver tumor tissues appear in different shapes, sizes, textures, contrast and number. Therefore various semi-automatic approaches mostly combining several methods have been proposed. The published work comprises graph cut followed by watershed for refined segmentation[91], adaptive multi-thresholding based on cross-entropy with level set techniques for segmentation refinement[92], bayesian classification with active contours refinement relying on manual selected seeds [93], Extreme Learning Machine (ELM) ensemble each trained on a random feature subspace of manually selected 3D samples in 3D[94], SVM for iterative 2D slice-per-slice pixel classification with morphological operations on manual selected tumor regions[95], SVM trained on user selected seeds for tumor extraction with corresponding feature vector based upon small regions produced by watershed transformations[96], online-learning probabilistic gray-level model based on user selected tumor regions with random walker to generate 3D segmentations [97], probability density functions modeled as a set of Gaussians with manual seeded 3D region growing[98], manual seeded 2D region growing utilizing size and shape constraints[99], and fuzzy c-means clustering on manual selected slices with segmentation refinement using hidden markov measure field models[100].

### 2.3. Public available liver and liver tumor datasets

Compared to other organs few research work on tumor segmentation in CT imaging has been focused on liver tumor segmentation so far. The lack of available, appropriate sized, and diligent annotated public datasets address the primary reason[12] . Available datasets are offer either a sparse number of images and ground truth segmentation or they are missing ground truth segmentations (Tab. 1).

Dataset	Institution	Liver	Tumor	Ground Truth	#Volumes	Modality	References
3Dircadb-01	IRCAD	✓	✓	✓	20	CT	[101]
3Dircadb-02	IRCAD	✓	✓	✓	2	CT	[101]
Sliver'07	MICCAI	✓	✗	✓	30	CT	[102]
TCGA-LIHC	TCIA	✓	✓	✗	1688	CT, MR, PT	[103, 104]
MIDAS	IMAR	✓	✓	✗	4	CT	[105]

Table 1: Overview of public available datasets of medical liver and liver tumor images.

### 2.4. Medical Image Segmentation Benchmarks

In the last decade benchmarks have played an increasingly important role in the medical image analysis community. Between 2010 and 2017 overall more than 90 medical imaging benchmarks have been organized. The most prominent tasks were segmentation, detection, classification and prediction tasks. For the years of 2018/19, already 39 known benchmarks have been started and/or announced.[106] Shared characteristics of benchmarks, also known as "challenges", are that independent individuals and groups optimize their methods based on an open available training dataset provided by the challenge organizer. The optimized methods are then applied to an test dataset. Therefore necessary conditions are set for a structured comparison and assessment of different methods.

Well established benchmarks often set guiding principles by the provided dataset and evaluation methods and therefore define a baseline for future improvements for certain medical imaging problems [107]. Furthermore, when new data is added to a benchmark dataset, annotation and evaluation protocols can be applied to ensure a consistent and continuous quality for future learning methods. The ground truth of the test dataset is stored privately on an online platform which provides automatic evaluation capabilities. This avoids inadvertent results by overtrained methods or by methods trained on wrong training and test data splits. Therefore a central evaluation instance ensures representative and comparable results.

Past medical imaging benchmarks focused on a wide variety of organs. Particularly assessing the heart region by (semi-)automated segmentation of arterial wall thickness[108], endocardial three-dimensional ultrasound[109], right ventricle[110], coronary lumen on computed tomography angiography[107], and the whole heart using multiple modalities[111]. Organ segmentation benchmarks further focused on prostate segmentation [112] and whole body segmentation in 3D medical images[113]. Few benchmarks concentrated on (semi-)

automatic lesion segmentation. Among them are, in particular, Brain tumors segmentation benchmarks with from multi-modal imaging data[114], from T1- and T2-weighted MRI scans[115][116]. Others focus on skin lesion analysis[117] and stroke lesion segmentation[118].

Three liver and liver tumor related Benchmarks have been offered so far. The Segmentation of the Liver (Sliver'07) was organized in conjunction with MICCAI 2007 and offered 30 CT volumes[102].<sup>2</sup> The Liver Tumor Segmentation Challenge (LTSC'08) was introduced as a part MICCAI 2008 workshop[119] 30 liver tumors from CT Volumes are used for this challenge.<sup>3</sup> The ImageCLEF liver CT benchmark offered 50 volumes including liver labels and liver lesion bounding boxes[120].<sup>4</sup>

---

<sup>2</sup>Results: <http://www.sliver07.org/results.php>, accessed: 13.01.2019

<sup>3</sup>Results: <http://mbi.dkfz-heidelberg.de/grand-challenge2007/sites/proceed.htm>, accessed: 13.01.2019

<sup>4</sup>Results: <https://www.imageclef.org/2015/liver>, accessed: 13.01.2019

### 3. Set-Up of the LiTS Benchmark

In order receive scientific state-of-the-art in automated liver and liver tumor segmentation methods, the LiTS Benchmark is organized in conjunction with the IEEE International Symposium on Biomedical Imaging (ISBI) 2017 and with the conference on Medical Image Computing and Computer Assisted Interventions (MICCAI) 2017. Compared to ISBI 2017 tasks for liver segmentation and tumor burden estimation are added for MICCAI 2017.

#### 3.1. The ISBI 2017 and MICCAI 2017 Benchmark Challenges

The first LiTS benchmark was organized on April 18, 2017 in Melbourne, Australia, in a workshop held as part of the IEEE ISBI 2017 conference. During Winter 2016/2017, participants were solicited through private e-mails as well as public e-mail lists, social media and the IEEE ISBI workshop announcements. Participants had to register at our online benchmarking system hosted on [www.codalab.com](http://www.codalab.com) and could download annotated training data and test data. They were asked to submit a four page summary of their algorithm after successful submission to the codalab plattform. Submissions were reviewed by the organizers and a final group of 17 participants for the ISBI and 26 participants for MICCAI were invited to contribute to the challenge and this work. The LiTS benchmarking dataset contains 201 computed tomography images of the abdomen. 194 CT scans contain liver lesions. The data was collected from seven academic and clinical institutions arround the world, including the Technical University of Munich Germany, Ludwig Maximilian University of Munich Germany, Radboudumc Netherlands, Polytechnique Montral and CHUM Research Center Canada, Tel Aviv University and Sheba Medical Center and The Hebrew University of Jerusalem and Hadassah University Medical Center Israel and IRCAD France. In particular the LiTS benchmark includes the public 3DIRCAD-B dataset in the training-set. The data was acquired with different scanners and scanning protocols. The examined patients suffered from primary to secondary liver tumor and metastases. The data had been manually annotated with two labels (liver and lesion) by a trained radiologists or oncologists. The quality of the test segmentations was verified by three experienced radiologists in an blinded review. The data has been split into 131 training and 70 test cases. The test cases were published without annotation. After publishing the test images the participants had to infer their submission segmentations for the test images. To participate in the benchmark the participants had to upload their submission segmentations to the online benchmarking platform accepted. The online benchmarking platform automatically computed performance scores. Of the 17 groups that participated in the benchmark at ISBI, five methods presented their work at the IEEE ISBI 2017 workshop in Melbourne. During the plenary discussions it became apparent that using only segmentation and surface metrics for lesions are not sufficient and do not account for missed lesions. We therefore introduced new detections metrics for the MICCAI 2017 benchmark, which measures precision and recall of detected lesions. A lesion is considered to be detected, if has at least 50% overlap with the ground truth segmentation. Furthermore, a new dice-score metric was introduced for the MICCAI 2017 benchmark, measuring the dice-score per volume to ensure that segmentation results of volumes containing small tumor areas be weighted equally to volumes with large tumor

ares for the final for the tumor segmentation discore. The second LiTS benchmark was held on September 14, 2017 in Quebec City, Canada as a MICCAI 2017 workshop. The LiTS MICCAI challenge introduced two new benchmark tasks of liver segmentation and tumor burden estimation. Participants had to register at a new codalab benchmark and were asked to describe their algorithm after submission to the MICCAI benchmark deadline, resulting in 27 teams submitting in the MICCAI benchmark. The training data and test data for the benchmark was identical to the ISBI benchmark. In comparison to ISBI, the MICCAI benchmark evaluate besides lesion segmentation performance also liver segmentation performance and accuracy in determining the tumor burden for each subject. The workshop at the MICCAI 2017 proceeded in a similar fashion to the ISBI edition: the TOP participating teams were invited to present their methods in short 20 minute presentations.

Altogether, we report four different test results from the two events: one summarizing the ISBI 2017 tumor segmentation results (Section 4.4), the second for MICCAI 2017 results on liver segmentation (Section 4.5.1), tumor segmentation results (Section 4.5.2) and automatic tumor detection and tumor burden evaluation (Section 4.5.2). However, our emphasis in this work lays on liver tumor segmentation.

### *3.2. The LiTS image dataset*

The image data for the LiTS challenge derives from several clinical sites including Ludwig Maximilian University of Munich, Radboud University Medical Center of Nijmegen, Polytechnique & CHUM Research Center Montral, Tel Aviv University, Sheba Medical Center, IRCCD Institute Strasbourg and Hebrew University of Jerusalem. The studied subjects suffer from diverse types of liver tumor diseases. Primary tumor disease such as HCC as well as secondary liver tumors and metastasis derived from colorectal, breast and lung cancer are present. The tumors have varying contrast enhancement such as hyper or hypo-dense contrast. The images represent a mix of pre- and post-therapy abdomen CT scans. The image data was acquired with different CT scanners and acquisition protocols. The image data is also very diverse with respect to resolution and image quality. The image resolution ranges from 0.56mm to 1.0mm in axial and 0.45mm to 6.0mm in z direction. Also the number of slices in z ranges from 42 to 1026. Some images contain imaging artifacts (e.g. metall artefacts), which are present in real life clinical data.

In the training set and test set of the liver volumes show a normal distribution and is similar to known distributions [121]. The number of tumors varies between 0 and 75. Table 2 shows a higher number of tumor occurrences in the test set compared to the training set. The size of the tumors vary between  $38\text{mm}^3$  and  $349\text{cm}^3$ . The average tumor-liver intensity difference is defined as the average absolute difference between the liver voxel HU values and the tumor voxel values. They vary between 0 and 98 and have a mean of 31.94 (SD=20) and a median of 29.61.

### *3.3. Expert Annotation of Tumor Structures*

The human rater ground truth segmentation was performed by trained radiologists at every clinical site and was a second time verified by experienced three radiologists in a

	Liver Size (cm <sup>3</sup> )		#Tumors		Tumor Size (cm <sup>3</sup> )		Tumor Size (cm <sup>3</sup> )	
	Train	Test	Train	Test	Train	Test	Train	Test
Median	1631.28	1654.38	3	5	2.49	5.40	29.61	34.02
Mean	1689.82	1775.58	6.93	9.41	17.56	14.42	31.94	35.72

Table 2: Characteristics of LiTS Training and Test Split

institution blinded verification test. The employed segmentation protocol defined the segmentation mask as unhealthy liver tissue including primary tumors, secondary tumors and metastasis. All data was converted to single .nii files.

From total 201 CT volumes, 131 were chosen randomly for training and 70 CT volumes for the test set. The split was performed in such a way to have the same clinical site distribution in training and test set. The participants could download training data from the LiTS Challenge website<sup>5</sup> including training reference data, The test data without ground truth segmentation is also available for download.

### 3.4. Online Evaluation Platform

A central element of the LiTS benchmark is its online evaluation tool. We used CoDaLab, which was developed at Stanford University and Microsoft Research. On CoDaLab participants can download annotated training and blinded test data, and upload their segmentations for the test cases. The system automatically evaluates the performance of the uploaded segmentation maps, and makes the overall performance available to the participant. Average scores for the different tasks of liver and lesion segmentation as well as tumor burden estimation are also reported online in a leader board. The LiTS benchmark data is publicly available at CoDaLab, allowing any team around the world to develop and test novel liver lesion segmentation algorithms. Ground truth segmentation files for the LiTS test data are hosted on the CoDaLab but their download is protected and not possible for participants. The users upload their segmentation results through a web-interface, review the uploaded segmentation and then choose to start an automatic evaluation process. The CoDaLab platform automatically identifies the ground truth corresponding to the uploaded segmentations. The evaluation of the different label overlap measures used to evaluate the quality of the segmentation (such as Dice scores) take approx. 2 minutes per volume. The overall segmentation results of the evaluation are automatically published on the CoDaLab leader board webpage and can be downloaded as a CSV file for further statistical analysis. Currently, the CoDaLab platform has evaluated more than 60,000 segmentations and recorded over 850 registered LiTS users. We used it to host both the training and test data, and to perform the evaluations of the ISBI and MICCAI challenges. Up-to-date ranking is available at CoDaLab for researchers to continuously monitor new developments and streamline improvements. The software that generates the comparison metrics between ground truth and user submissions is available as the open source at [github.com<sup>6</sup>](https://github.com/PatrickChrist/LiTS-CHALLENGE).

<sup>5</sup>[www.lits-challenge.com](http://www.lits-challenge.com)

<sup>6</sup><https://github.com/PatrickChrist/LiTS-CHALLENGE>

### 3.5. Evaluation Metrics and Ranking

We assessed both the detection and the segmentation performance of the LiTS submissions. The tasks of detection and segmentation are closely linked; segmentation of lesions requires their detection. Thus, some metrics evaluate both simultaneously (see section 3.5.1 "Mixed metrics"). In an effort to evaluate detection and segmentation separately, we prepared a set of detection metrics and a set of segmentation metrics. The detection metrics are presented in section 3.5.2 "Detection metrics". The segmentation metrics are evaluated on liver and only on those lesions that are detected; these are presented in section 3.5.3 "Segmentation metrics".

#### 3.5.1. Mixed metrics

There are two related metrics that jointly evaluate detection and segmentation performance, based on the Dice score. The Dice score is an F1 score which measures the harmonic mean of precision and recall, in this case for binary pixel classification. This score is essentially a per-pixel detection score. When applied to a binary segmentation task, it evaluates the degree of overlap between the predicted segmentation mask and the reference segmentation mask. Given binary masks  $A$  and  $B$ , the Dice score evaluates as:

$$DICE(A, B) = \frac{2|A \cap B|}{|A| + |B|}. \quad (1)$$

in the interval  $[0,1]$ ; a perfect segmentation yields a Dice score of 1.

Poor segmentation manifests in a poor overlap as measured by the Dice score. For lesion segmentation, the success of lesion detection also impacts the Dice score though not in an ideal manner. False positive and false negative lesion predictions impart a penalty in terms of the erroneous overlap of the prediction with the reference mask. However, this penalty depends on the relative size of the erroneous lesion with respect to the collective sizes of rest of the predicted and reference lesions. Thus, failing to predict a nodular lesion is much more costly in a volume with no other lesions than in a volume with many lesions or with another large lesion. In section 3.5.3, we separate the Dice score from lesion detection by evaluating it only for each detected lesion, as a segmentation metric.

As a mixed segmentation and detection metric, we evaluate the Dice score in two ways. First, as a **global Dice** score, applied across all cases as if they combine in a single volume. Second, as a Dice score applied per case (**Dice per case**) and averaged over all cases. The global Dice score is affected more by large lesions than by small lesions. The Dice per case score applies a higher penalty to prediction errors in cases with fewer actual lesions. Despite the drawbacks of these metrics, they are fairly informative; nevertheless, we also compute a host of other metrics to better understand detection and segmentation performance.

#### 3.5.2. Detection metrics

A lesion is considered detected if the predicted lesion has a sufficient overlap with its corresponding reference lesion, measured as the intersection over union of their respective segmentation masks. This allows for a count of true positive, false positive, and false negative detections, from which we compute the **precision** and **recall** of lesion detection. Detection

performance is evaluated at intersection over union greater than 0 as well as greater than 0.5, with the former being the most sensitive.

Since lesions are not predicted for one reference lesion at a time, a correspondence between reference lesions and predictions must be established. Connected components are identified in both the prediction mask and the reference mask. Components may not necessarily have a one-to-one correspondence between the two masks. A single reference component can be predicted as multiple components (split error); similarly, multiple reference components can be covered by a single large predicted component (merge error). As a first step, the detection algorithm turns this many-to-many mapping into a many-to-one mapping by merging all reference lesions that are connected by predicted components. Thus, a single corresponding (merged) reference component is found for every predicted component (except those that do not overlap any reference component). Before evaluating intersection over union, all predicted components that correspond to the same reference component are merged. In order to maintain the immutability of the reference, detection of any merged components in the reference masks counts for the number of lesions merged.

### 3.5.3. Segmentation metrics

We evaluated the quality of segmentation of the liver and of detected lesions (at intersection over union greater than 0.5). These include overlap measures and surface distance metrics. Of the four overlap measures, three are reformulations of the same measurement: **Dice** score, **Jaccard** index, and volume overlap error (**VOE**). The Dice score is measured for each detected lesion as in equation 1. The Jaccard index is the intersection over union of the predicted lesion mask with the reference lesion mask. Volume overlap error is the complement of the Jaccard index:

$$VOE(A, B) = 1 - \frac{|A \cap B|}{|A \cup B|}. \quad (2)$$

The relative volume difference (**RVD**) is an asymmetric measure defined as:

$$RVD(A, B) = \frac{|B| - |A|}{|A|}. \quad (3)$$

Surface distance metrics are a set of correlated measures of the distance between the surfaces of a reference and predicted lesion.

Let  $S(A)$  denote the set of surface voxels of  $A$ . The shortest distance of an arbitrary voxel  $v$  to  $S(A)$  is defined as:

$$d(v, S(A)) = \min_{s_A \in S(A)} \|v - s_A\|, \quad (4)$$

where  $\|\cdot\|$  denotes the Euclidean distance. The average symmetric surface distance (**ASD**) is then given by:

$$ASD(A, B) = \frac{1}{|S(A)| + |S(B)|} \left( \sum_{s_A \in S(A)} d(s_A, S(B)) + \sum_{s_B \in S(B)} d(s_B, S(A)) \right). \quad (5)$$

The maximum symmetric surface distance (**MSD**), also known as the Symmetric Hausdorff Distance, is similar to ASD except that the maximum distance is taken instead of the average:

$$MSD(A, B) = \max \left\{ \max_{s_A \in S(A)} d(s_A, S(B)), \max_{s_B \in S(B)} d(s_B, S(A)) \right\}. \quad (6)$$

### 3.5.4. Tumor burden

The tumor burden of the liver is a measure of the fraction of the liver afflicted by cancer. As a metric, we measure the root mean square error (RMSE) in tumor burden estimates from lesion predictions.

$$RMSE = \sqrt{\frac{1}{n} \sum_{i=1}^n (A_i - B_i)^2} \quad (7)$$

## 4. Results

In a first step we give an overview and describe the main characteristics of submitted approaches. Further we analyze the performance of participants who a short paper and described their submitted methods for ISBI(2017) and MICCAI(2017).

### 4.1. Overview

In total, the LiTS challenge received 61 valid submissions and 26 contributing short-papers as part of the two workshops at ISBI and MICCAI. Out of these, 18 included 4-page short papers detailing their employed methods (see Appendix). Outside of the core workshops, the test data set was downloaded 262 times and 367 participants from 25 countries were recorded with the USA, China and Germany being the most frequently represented countries. This paper focuses on submissions received during the two workshops.

The highest global Dice scores over both challenges were in the low .80 range for the tumor segmentation task and in around .96 for liver segmentation. The overall best tumor segmentation global Dice value was achieved by Li et al. with 0.829 followed by Yuan et al. with 0.820. While the usage of different metrics did maintain the global Dice score dependent ranking order to some extent with some metrics, we observed considerable variation of ranking order in other metrics and for individual submissions. This high dependence of the ranking on the metric used was especially pronounced in the MICCAI submissions and on an individual level. On average, methods showed higher performance on the MICCAI workshop compared to the ISBI workshop.

### 4.2. Main characteristics of submitted approaches

All but one submission provided a fully automatic segmentation approach and all but two methods relied on supervised learning. Two approaches focused solely on the tumor segmentation task while all other generated both a liver and tumor segmentation result. A U-Net derived architecture was overwhelmingly used in the challenge with only two automated methods using a modified VGG-net (Qi et al.) and a k-CNN (Lipkova et al.) respectively. In the majority of the submissions multiple U-nets were cascaded with each net focusing solely on liver segmentation, tumor segmentation or a performance enhancing supplementary task. Additional residual connections and adjusted input resolution were the most common changes to the basic U-Net architecture. Three submissions combined individual models as an ensemble technique. 3D methods were not directly employed on the original image data by any of the methods. However, some techniques allowed three-dimensional convolutions in a secondary role specializing on solely the tumor segmentation task with smaller input resolution images. Instead of full 3D, other methods tried to capture the advantages of three-dimensionality by using a 2.5 D model architecture, i.e. providing a stack of images as a multi-channel input to the network and receiving the segmentation mask of the center slice of this stack as a network output.

The most common optimizers varied between ADAM and Stochastic gradient descent with momentum with one approach relying on RMSProp. Multiple different loss functions were used for training including standard and class-weighted cross entropy, Dice loss, Jaccard

loss, Tversky loss, L2 loss as well as ensemble loss techniques combining multiple individual loss functions into one.

Almost all methods employed some form of data pre-processing with HU-value clipping, normalization and standardization being the most frequent techniques. Data augmentation was also widely used and was for the most part focused on standard geometric transformations such as flipping, shifting, scaling or rotation. Some more advanced techniques such as histogram equalization and random contrast normalization were implemented by individual submissions.

Some type of post-processing was also used by the vast majority of methods. The common post-processing steps were to form connected lesion components and to overlay the liver mask on the lesion segmentation to discard any lesions located outside the liver region. More advanced methods included a Random Forest classifier, morphological filtering, a special shallow neural network to eliminate false positive or custom algorithms for lesion hole filling.

#### *4.3. Synthetic Fusion algorithms*

Four fusion algorithms evaluated on the global dice score and dice score per case have been evaluated. The four fusion algorithms select the best segmentation results per volume shown in figures 3, 6 and 7 in as gray plots. The best performing fusion approach both for ISBI and MICCAI is based on all submissions (best\_all\_vol). Further fusion algorithms are based on all automatic segmentation methods (no\_human\_vol), the best five (best\_5\_vol) and the best two (best\_2\_vol).

#### *4.4. Performance of algorithms at ISBI*

A total of 13 groups participated in the ISBI challenge out of which 11 supplied a short paper summary of their work. Participants were ranked according to the main metric global Dice score with regards to their performance in the lesion segmentation task (Fig 1). Four other metrics, namely VOE, RVD, ASD and MSD were recorded for each method as well. The highest Dice scores were in the middle .60s range with Han achieving a score of .67 closely followed by Vorontsov and Chlebius with a Dice value of 0.65 and Bi with 0.64. The ranking changes to some degree when considering other metrics with for example Maninis obtaining the third best RVD score but overall retains its order with the best methods according to Dice also generally performing better at other metrics. One exception to this observation was the work by Ma who supplied an interactive method compared to the fully automated submissions of all other participants.

Regarding their architecture, the best performing methods used mostly cascaded U-Net approaches with short and long skip connections and 2.5D input images being among the most beneficial features. In addition, weighted cross entropy loss functions as well as a few ensemble learning techniques were employed by most of the winning methods together with some common pre- and post-processing steps such as HU-value clipping and connected component labeling respectively.

Ranking	Name	Institution	VOE	RVD	ASD	MSD	Dice per case
1	X. Han	Elekta Inc.	0,45	0,04	6,66	57,93	67
2	E. Vorontsov et al.	MILA	0,47	-0,21	7,12	51,96	65
2	G. Chlebus et al.	Fraunhofer	0,46	17,41	17,75	57,64	65
3	L. Bi et al.	Uni Sydney	0,46	1,9	21,19	72,8	64
4	C. Wang et al.	KTH Sweden	0,54	3,93	26,02	85,38	58
6	J. Lipkova et al.	TU Munich	0,63	103,31	32,32	105,82	48
7	J. Ma et al.	NJUST	0,65	-0,35	11,49	64,31	47
9	T. Konopczynski et al.	Uni Heidelberg	0,69	103,74	32,54	116,6	42
10	M. Beliver	ETH Zurich	0,69	3,6	36,29	130,46	41
11	K. Maninis	ETH Zurich	0,71	1,23	19,74	86,83	38
12	J. Qi et al.	UESTC	0,87	1985,2	40,61	95,63	19

Table 3: Table ISBI lesion submissions ranked by Dice per case score. \* indicates missing short paper submission

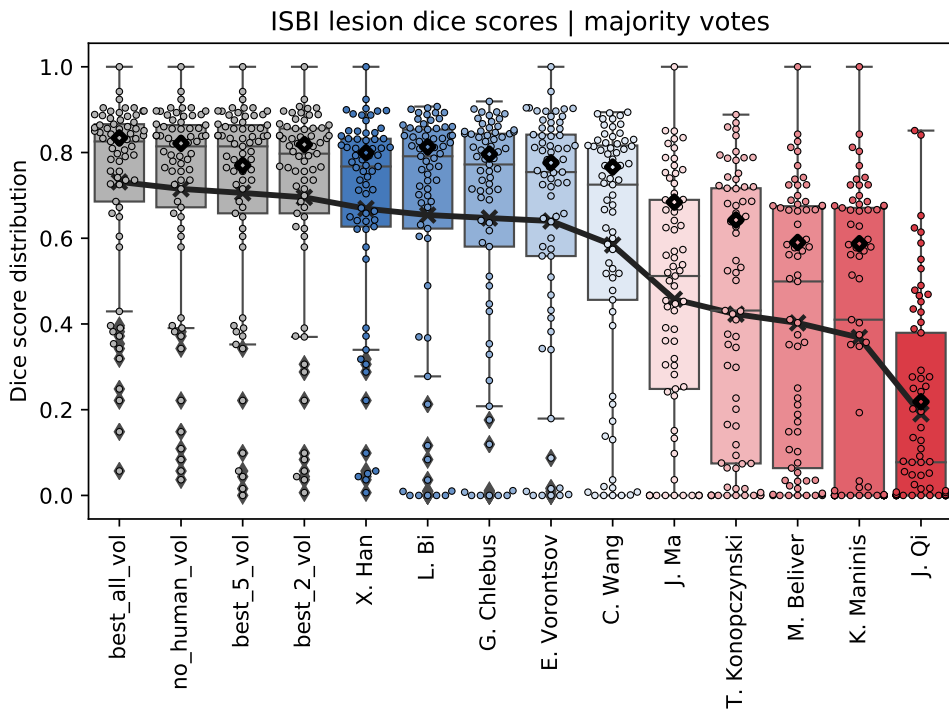


Figure 3: Dispersion of test Dice scores from individual algorithms described in short-papers, and various fused algorithmic segmentations (gray). Boxplots show quartile ranges of the scores on the test datasets; whiskers and dots indicate outliers. Black squares indicate the global dice metric whereas the black line indicates the ranking based on the dice per case metric. Also shown are results of four fused algorithmic segmentations.

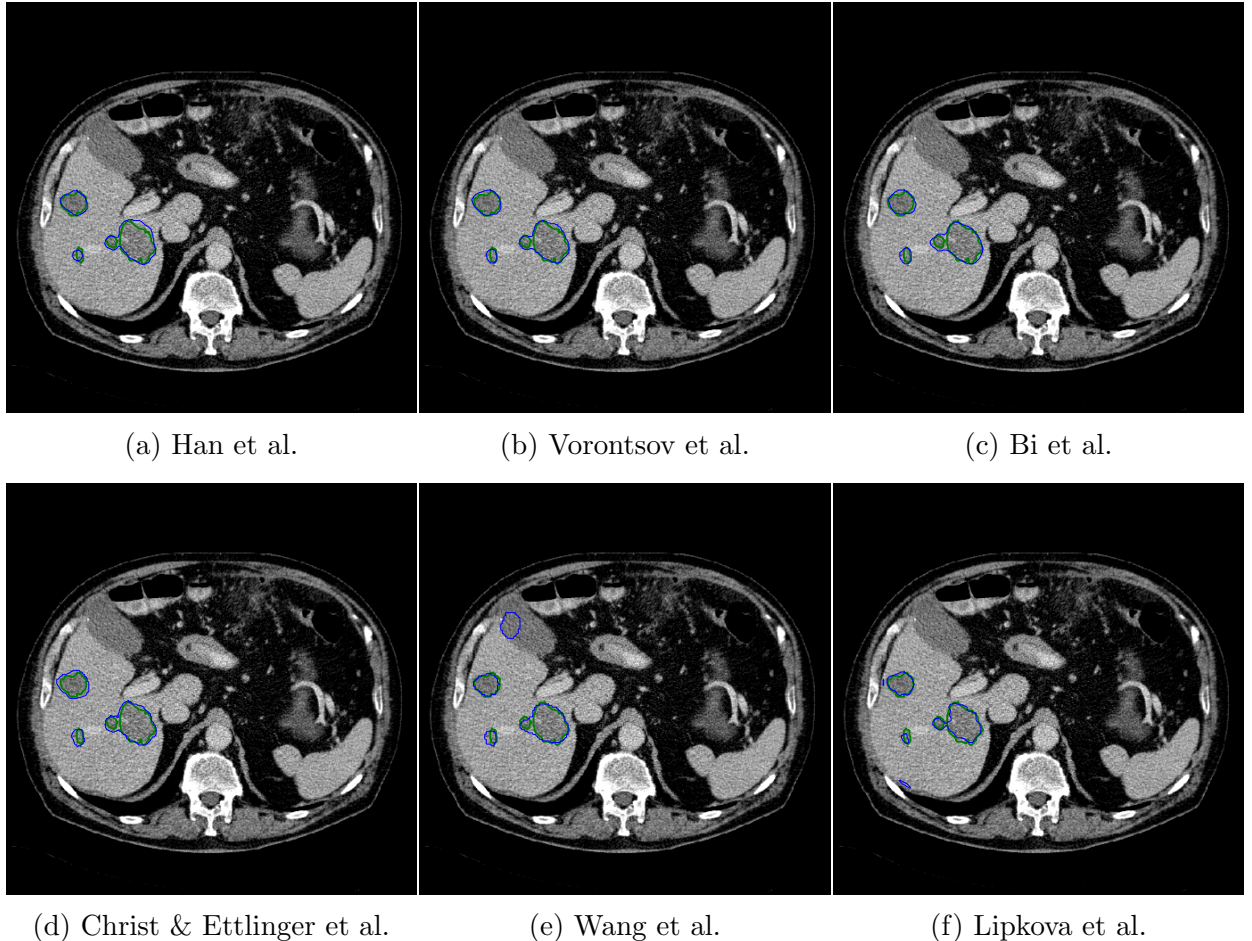


Figure 4: Lesion segmentation results of the LiTS ISBI challenge. Volume 68 slice 262

#### 4.5. Performance of algorithms at MICCAI

The MICCAI challenge received a total of 28 submissions out of which 15 were described with a short paper. Methods were ranked in the four different tasks of lesion segmentation, liver segmentation, LiTS detection and tumor burden and 10 different metrics were used among the four tasks. The best lesion segmentation Dice scores improved significantly with respect to ISBI with MICCAI’s highest global Dice having a value of 0.829 compared to ISBI’s 0.670 (Table 2). However the best MICCAI method according to the newly introduced Dice per case coefficient scored 0.702 and therefore significantly lower than the highest global Dice score.

In general, the winning submissions integrated the learnings from the ISBI workshop into their methods and improved them accordingly. Therefore, the main architectural differences compared to the ISBI submissions were the higher usage of ensemble learning methods, a higher incidence of residual connections and an increased number of more sophisticated post-processing steps with both custom algorithms, morphological filtering operations and special classifiers such as Random Forests or shallow neural networks being utilized.

Ranking	Name	Institution	RMSE	Max Error
1	Li et al.	CUHK	0.0150 (1)	0.0620 (8)
2	Wu et al.	NJU	0.0160 (2)	0.0480 (4)
2	Wang et al.	KTH	0.0160 (2)	0.0580 (6)
3	Yuan et al.	MSSM	0.0170 (3)	0.0490 (5)
3	Tian et al.	Lenovo	0.0170 (3)	0.0450 (3)
4	Kaluva et al.	Predible Health	0.0200 (4)	0.0900 (14)
4	Han	ELEKTA	0.0200 (4)	0.0800 (12)
4	Ben-Cohen et al.	Uni Tel Aviv	0.0200 (4)	0.0700 (10)
4*	jrwin	N.A.	0.0200 (4)	0.0860 (13)
4	Chlebus et al.	Fraunhofer	0.0200 (4)	0.0700 (10)
5*	LP777	N.A.	0.0220 (5)	0.0740 (11)
6	Vorontsov et al.	MILA	0.0230 (6)	0.1120 (17)
6*	jkan	N.A.	0.0230 (6)	0.0680 (9)
6*	szm0219	Uni Illinois	0.0230 (6)	0.0940 (16)
7*	huni1115	N.A.	0.0260 (7)	0.1160 (18)
7*	MICDIIR	N.A.	0.0260 (7)	0.0450 (3)
8*	Micro	N.A.	0.0270 (8)	0.0610 (7)
9	Lipkova et al.	TU Munich	0.0300 (9)	0.1400 (19)
9	Roth et al.	Volume Graphics	0.0300 (9)	0.1800 (21)
10	Piraud et al.	TU Munich	0.0370 (10)	0.1430 (20)
11*	NMIP_HQU	N.A.	0.0400 (11)	0.1400 (19)
12*	jinqi	N.A.	0.0420 (12)	0.0330 (2)
13*	mahendrakhened	IITM	0.0440 (13)	0.1940 (22)
14*	mbb	ETH Zurich	0.0540 (14)	0.0920 (15)
15	Bi et al.	Uni Sydney	0.1700 (15)	0.0740 (11)
16	Ma et al.	NJUST	0.9200 (16)	0.0610 (7)
17*	QiaoTian	N.A.	0.9500 (17)	-0.6500 (1)

Table 4: Table MICCAI submissions tumor burden ranking. \* indicates missing short paper submission

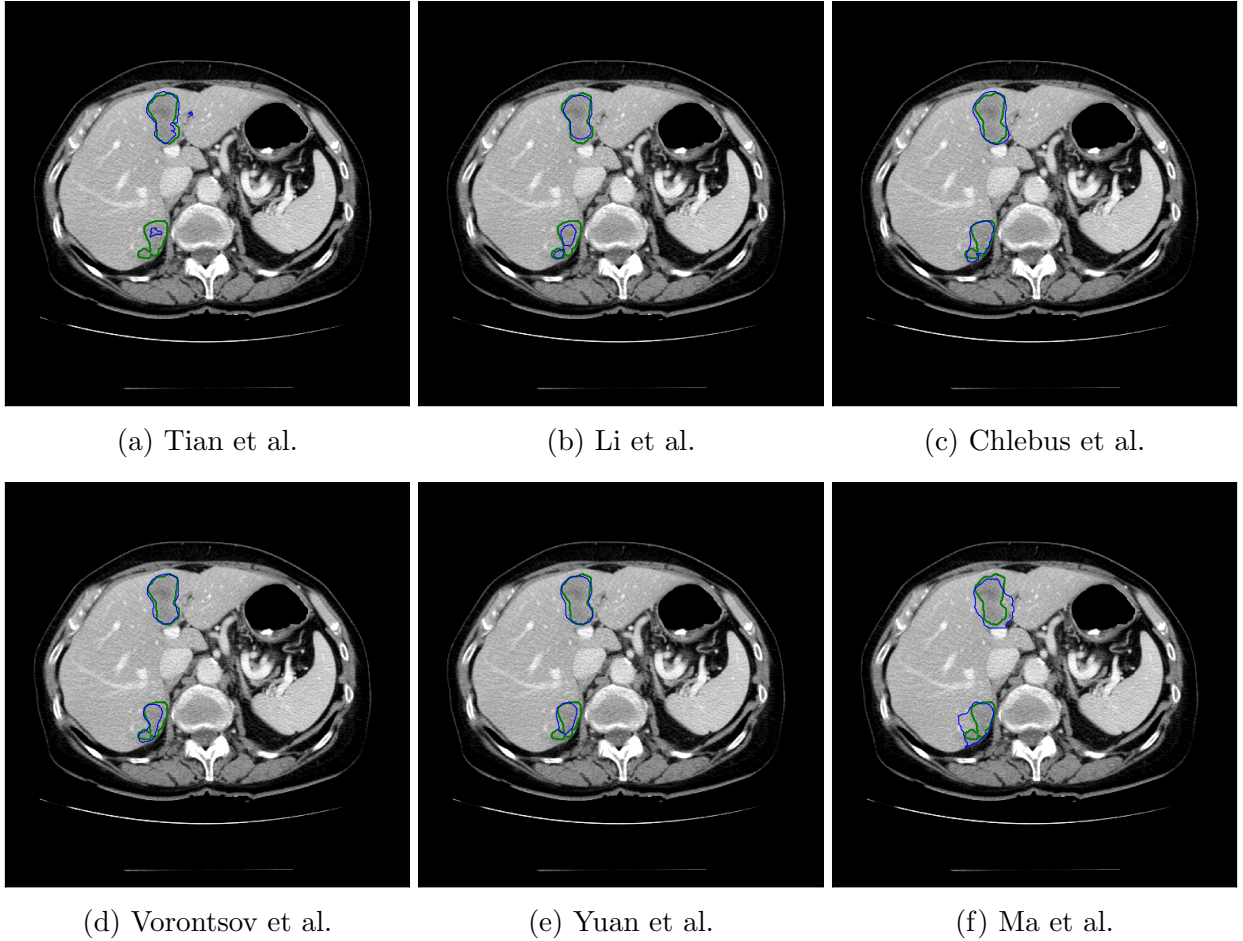


Figure 5: Lesion segmentation results of the LiTS MICCAI challenge. Volume 49 slice 60

#### 4.5.1. MICCAI liver segmentation

The evaluation of the liver segmentation task relied on all seven metrics explained in the previous chapter with the Dice score per case acting as the main metric used for the final ranking (Tab. 5). Almost all methods except the last three achieved Dice per case values of above 0.920 with the best one scoring 0.970. Ranking positions remain relatively stable when ordering submissions according to the other overlap metrics Dice global and VOE with most methods only changing by a few spots and the top four methods only interchanging positions among themselves. The position variation is larger when using the surface distance metrics ASSD, MSD and RMSD as a basis for the ranking with some methods moving up to 8 positions. However on average, the best performing Dice per case methods still also achieve the lowest surface distance values with the winning method retaining the top spot in all rankings. The highest variation of results is observed by the RVD metric where little correlations with the Dice per case ranking positions remains.

Ranking	Name	Institution	Dice per case	Dice global	VOE	RVD	ASSD	MSD	RMSD
1	Yuan et al.	MSSM	0.9630 (1)	0.9670 (2)	0.071 (2)	-0.010 (9)	1.104 (1)	23.847 (1)	2.303 (1)
2	Tian et al.	Lenovo	0.9610 (2)	0.9640 (4)	0.075 (4)	0.023 (17)	1.268 (4)	27.016 (4)	2.776 (4)
2	Li et al.	CUHK	0.9610 (2)	0.9650 (3)	0.074 (3)	0.000 (14)	1.692 (9)	29.411 (8)	3.729 (10)
3	Ben-Cohen et al.	Uni Tel Aviv	0.9600 (3)	0.9700 (1)	0.070 (1)	0.000 (14)	1.130 (2)	24.450 (2)	2.390 (2)
3	Chlebus et al.	Fraunhofer	0.9600 (3)	0.9650 (3)	0.077 (6)	-0.004 (13)	1.150 (3)	24.499 (3)	2.421 (3)
3*	LP777	N.A.	0.9600 (3)	0.9630 (5)	0.076 (5)	0.009 (15)	1.510 (8)	31.225 (10)	3.510 (8)
4	Wu et al.	N.A.	0.9590 (4)	0.9630 (5)	0.079 (7)	-0.009 (10)	1.311 (5)	28.229 (6)	2.929 (5)
5*	jrwin	N.A.	0.9580 (5)	0.9620 (6)	0.081 (9)	-0.016 (8)	1.360 (6)	27.732 (5)	2.994 (6)
5	Wang et al.	KTH	0.9580 (5)	0.9620 (6)	0.080 (8)	-0.006 (12)	1.367 (7)	32.933 (14)	3.260 (7)
6*	MICDIIR	N.A.	0.9560 (6)	0.9590 (7)	0.083 (10)	0.031 (18)	1.847 (11)	35.653 (16)	4.393 (15)
7	Vorontsov et al.	MILA	0.9510 (7)	0.9510 (10)	0.093 (12)	-0.009 (10)	1.785 (10)	29.769 (9)	3.933 (13)
8	Kaluva et al.	Predictive Health	0.9500 (8)	0.9500 (11)	0.090 (11)	-0.020 (7)	1.880 (13)	32.710 (13)	4.200 (14)
8	Roth et al.	Volume Graphics	0.9500 (8)	0.9400 (14)	0.100 (13)	-0.050 (6)	1.890 (14)	31.930 (12)	3.860 (12)
9*	hun1115	N.A.	0.9460 (9)	0.9470 (12)	0.101 (14)	-0.009 (10)	1.869 (12)	31.840 (11)	3.788 (11)
10	Han	N.A.	0.9400 (10)	0.9400 (14)	0.110 (15)	0.050 (19)	2.890 (17)	51.220 (18)	7.210 (17)
10	Lipkova et al.	TU Munich	0.9400 (10)	0.9400 (14)	0.120 (17)	0.060 (20)	3.540 (20)	186.250 (25)	11.240 (23)
11*	mbb	ETH Zurich	0.9380 (11)	0.9520 (9)	0.113 (16)	-0.006 (12)	2.900 (18)	90.245 (21)	7.902 (19)
12	Bi et al.	Uni Sydney	0.9340 (12)	0.9580 (8)	0.101 (14)	257.163 (23)	258.598 (27)	321.710 (26)	261.866 (27)
13*	Micro	N.A.	0.9320 (13)	0.9410 (13)	0.126 (18)	0.088 (21)	2.182 (16)	33.588 (15)	4.501 (16)
14*	MIP_HQU	N.A.	0.9300 (14)	0.9400 (14)	0.120 (17)	0.010 (16)	2.160 (15)	29.270 (7)	3.690 (9)
14*	szm0219	Uni Illinois	0.9300 (14)	0.9410 (13)	0.126 (18)	-0.068 (4)	3.974 (21)	61.894 (19)	9.136 (20)
15*	jinqi	N.A.	0.9240 (15)	0.9230 (17)	0.140 (19)	-0.052 (5)	5.104 (23)	123.332 (23)	13.464 (24)
16*	mahendrakhened	IITM	0.9120 (16)	0.9230 (17)	0.150 (20)	-0.008 (11)	6.465 (24)	45.928 (17)	9.682 (21)
18*	jkan	N.A.	0.9060 (18)	0.9390 (15)	0.157 (21)	-0.107 (2)	3.367 (19)	63.232 (20)	7.847 (18)
19	Piraud et al.	TU Munich	0.7670 (19)	0.7790 (18)	0.371 (22)	0.606 (22)	37.450 (26)	326.334 (27)	70.879 (26)
20*	QiaoTian	N.A.	0.0500 (20)	0.0600 (20)	0.970 (23)	-0.970 (1)	31.560 (25)	90.470 (22)	36.800 (25)
21	Ma et al.	NJUST	0.0410 (21)	0.1350 (19)	0.973 (24)	8229.525 (24)	8231.318 (28)	8240.644 (28)	8232.225 (28)

Table 5: Table MICCAI liver submissions ranked by Dice per case score. \* indicates missing short paper submission

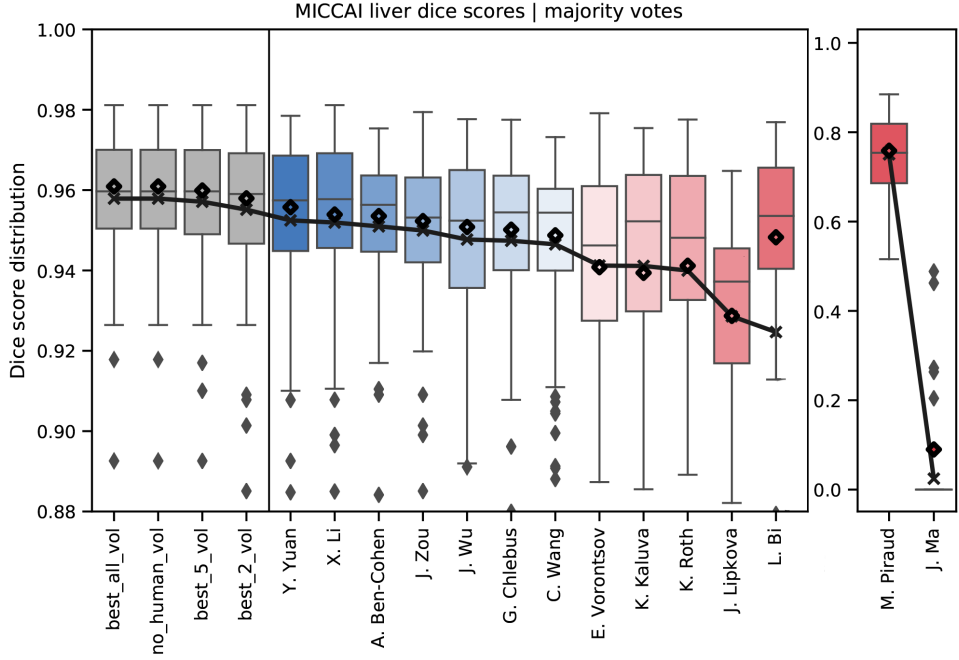


Figure 6: Dispersion of test Dice scores from individual algorithms described in short-papers, and various fused algorithmic segmentations (gray). Boxplots show quartile ranges of the scores on the test datasets; whiskers and dots indicate outliers. Black squares indicate the global dice metric whereas the black line indicates the ranking based on the dice per case metric. Also shown are results of four "fused algorithmic segmentations".

#### 4.5.2. MICCAI liver tumor segmentation

Compared to the lesion segmentation at ISBI two new metrics, namely RMSD and Dice per case were added with the latter acting as the new main metric to derive a ranking of methods. The Dice score used as a main metric previously was still recorded but renamed to global Dice to avoid confusion while maintaining comparability. The best-performing Dice per case methods obtained values in the high .60s with the winning method even surpassing the 0.7 threshold with a final score of .702.

Compared to the liver segmentation task there is an overall positive correlation of ranking positions with submissions that performed well at liver segmentation on average also obtaining good results at the lesion segmentation task with some exceptions such as Ma et al. whose method changed by 20 positions. Considering the lesion segmentation rankings according to other metrics, a weak positive correlation between the Dice per case ranking and the three surface distance metrics ASSD, MSD and RMSD as well as the Dice global metric can still be observed, although a considerable portion of methods change positions by more than a few spots depending on the evaluation metric. The ranking according to VOE shows very little correlation with the Dice per case results, while RVD implies a negative correlation with many methods that performed bad with respect to the Dice per case metric achieving top ranking positions.

The lesion detection metrics showed a positive correlation with the Dice per case ranking (Tab. 7). Out of the best 7 methods according to Dice per case, 6 were also in the top 7 in the precision at 50% overlap ranking and 5 were also in the top 7 in the recall at 50% overlap method. However, there were also considerable position changes with some of the most extreme being the 1st Dice per case method finishing 14th in precision and the 16th Dice per case method finishing first according to the recall method.

The tumor burden was very well predicted by many methods with the best performing methods achieving a lowest RMSE of 0.0150 and a lowest maximum error at 0.0330 (Tab. ??). There was little variation in RMSE values apart from the last two or three methods with even the 19th method still obtaining the 9th rank due to the high number of duplicates in the low range of values. On average methods achieving high Dice per case scores also obtained lower RMSE values. Only a smaller correlations exists between RMSE and the maximum error ranking.

In general, a larger liver lesion volume facilitated the lesion segmentation task across all methods (Fig. 6 a)). Similarly, an average lesion-liver HU difference between -10 and -60 resulted in considerably better average lesion segmentation performance than both higher and lower difference values (Fig 6 b)). The median difference value among all slices was thereby at around -35.

#### 4.6. Overall Segmentation performance

In total, the liver segmentation task was performed very well with Dice scores in the high .90s while the liver lesion segmentation task achieved scores in the low .70s thereby

Ranking	Name	Institution	Dice per case	Dice global	VOE	RVD	ASSD	MSD	RMSD
1	Tian et al.	Lenovo	0.7020 (1)	0.7940 (5)	0.394 (11)	5.921 (18)	1.189 (12)	6.682 (5)	1.726 (8)
2	Li et al.	CUHK	0.6860 (2)	0.8290 (1)	0.356 (3)	5.164 (17)	1.073 (5)	6.055 (1)	1.562 (2)
3	Chlebus et al.	Fraunhofer	0.6760 (3)	0.7960 (4)	0.383 (10)	0.464 (12)	1.143 (8)	7.322 (12)	1.728 (9)
4	Vorontsov et al.	MILA	0.6610 (4)	0.7830 (9)	0.357 (4)	12.124 (24)	1.075 (6)	6.317 (3)	1.596 (3)
5	Yuan et al.	MSSM	0.6570 (5)	0.8200 (2)	0.378 (9)	0.288 (11)	1.151 (9)	6.269 (2)	1.678 (5)
6	Ma et al.	NJUST	0.6550 (6)	0.7680 (12)	0.451 (19)	5.949 (19)	1.607 (24)	9.363 (25)	2.313 (24)
7	Bi et al.	Uni Sydney	0.6450 (7)	0.7350 (16)	0.356 (3)	3.431 (13)	1.006 (2)	6.472 (4)	1.520 (1)
8	Kaluvu et al.	Predible Health	0.6400 (8)	0.7700 (11)	0.340 (1)	0.190 (9)	1.040 (3)	7.250 (11)	1.680 (6)
9	Han	N.A.	0.6300 (9)	0.7700 (11)	0.350 (2)	0.170 (8)	1.050 (4)	7.210 (9)	1.690 (7)
10	Wang et al.	KTH	0.6250 (10)	0.7880 (7)	0.378 (9)	8.300 (21)	1.260 (15)	6.983 (8)	1.865 (13)
11	Wu et al.	N.A.	0.6240 (11)	0.7920 (6)	0.394 (11)	4.679 (14)	1.232 (14)	7.783 (17)	1.889 (14)
12	Ben-Cohen et al.	Uni Tel Aviv	0.6200 (12)	0.8000 (3)	0.360 (5)	0.200 (10)	1.290 (16)	8.060 (19)	2.000 (16)
12*	LP777	N.A.	0.6200 (12)	0.8000 (3)	0.421 (14)	6.420 (20)	1.388 (20)	6.716 (6)	1.936 (15)
13*	Micro	N.A.	0.6130 (13)	0.7830 (9)	0.430 (16)	5.045 (16)	1.759 (27)	10.087 (26)	2.556 (25)
13*	Njirwin	N.A.	0.6130 (13)	0.7640 (13)	0.361 (6)	4.993 (15)	1.164 (11)	7.649 (15)	1.831 (12)
14*	mbb	ETH Zurich	0.5860 (14)	0.7410 (15)	0.429 (15)	39.763 (27)	1.649 (26)	8.079 (20)	2.252 (23)
15*	szm0219	Uni Illinois	0.5850 (15)	0.7450 (14)	0.364 (7)	0.001 (4)	1.222 (13)	7.408 (13)	1.758 (10)
16*	MICDIIR	N.A.	0.5820 (16)	0.7760 (10)	0.446 (18)	8.775 (22)	1.588 (23)	7.723 (16)	2.182 (22)
17	Roth et al.	Volume Graphics	0.5700 (17)	0.6600 (20)	0.340 (1)	0.020 (5)	0.950 (1)	6.810 (7)	1.600 (4)
18*	jkan	N.A.	0.5670 (18)	0.7840 (8)	0.364 (7)	0.112 (7)	1.159 (10)	7.230 (10)	1.690 (7)
19*	huni1115	N.A.	0.4960 (20)	0.7000 (18)	0.400 (12)	0.060 (6)	1.342 (19)	9.030 (24)	2.041 (17)
20*	mahendrakhened	IITM	0.4920 (21)	0.6250 (23)	0.411 (13)	19.705 (26)	1.441 (21)	7.515 (14)	2.070 (19)
21	Lipkova et al.	TU Munich	0.4800 (22)	0.7000 (18)	0.360 (5)	0.060 (6)	1.330 (17)	8.640 (22)	2.100 (20)
22*	jinqi	N.A.	0.4710 (23)	0.6470 (22)	0.514 (20)	17.832 (25)	2.465 (28)	14.588 (28)	3.643 (27)
23*	MIP_HQU	N.A.	0.4700 (24)	0.6500 (21)	0.340 (1)	-0.130 (1)	1.090 (7)	7.840 (18)	1.800 (11)
24	Piraud et al.	TU Munich	0.4450 (25)	0.6960 (19)	0.445 (17)	10.121 (23)	1.464 (22)	8.391 (21)	2.136 (21)
25*	QiaoTian	N.A.	0.2500 (26)	0.4500 (24)	0.370 (8)	-0.100 (2)	1.620 (25)	11.720 (27)	2.620 (26)

Table 6: Table MICCAI lesion submissions ranked by Dice per case score. \* indicates missing short paper submission

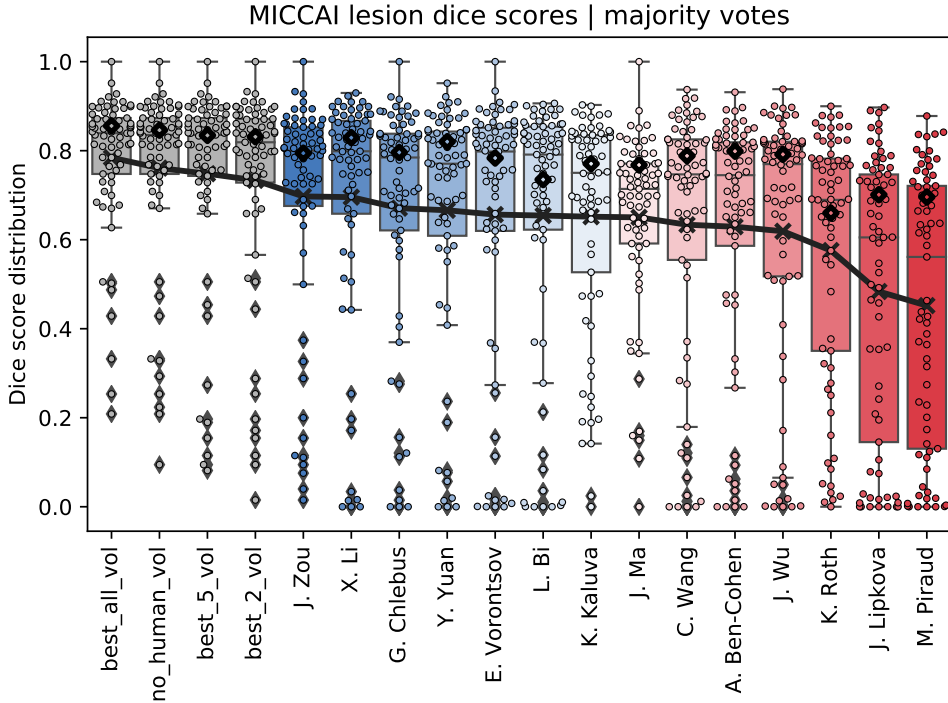


Figure 7: Dispersion of test Dice scores from individual algorithms described in short-papers, and various fused algorithmic segmentations (gray). Boxplots show quartile ranges of the scores on the test datasets; whiskers and dots indicate outliers. Black squares indicate the global dice metric whereas the black line indicates the ranking based on the dice per case metric. Also shown are results of four fused algorithmic segmentations.

Ranking	Name	Institution	Precision at 50% overlap	Recall at 50 % overlap
1	Tian et al.	Lenovo	0.156 (14)	0.437 (3)
2	Li et al.	CUHK	0.409 (4)	0.408 (4)
3	Chlebus et al.	Fraunhofer	0.496 (2)	0.397 (5)
4	Vorontsov et al.	MILA	0.446 (3)	0.374 (6)
5	Yuan et al.	MSSM	0.328 (5)	0.397 (5)
6	Ma et al.	NJUST	0.499 (1)	0.289 (17)
7	Bi et al.	Uni Sydney	0.315 (6)	0.343 (11)
8	Kaluva et al.	Predible Health	0.140 (16)	0.330 (12)
9	Han	N.A.	0.160 (13)	0.330 (12)
10	Wang et al.	KTH	0.160 (13)	0.349 (9)
11	Wu et al.	N.A.	0.179 (12)	0.372 (7)
12	Ben-Cohen et al.	Uni Tel Aviv	0.270 (7)	0.290 (16)
12*	LP777	N.A.	0.239 (9)	0.446 (2)
13*	Micro	N.A.	0.095 (19)	0.328 (13)
13*	jrwin	N.A.	0.241 (8)	0.290 (16)
14*	mbb	ETH Zurich	0.054 (23)	0.369 (8)
15*	szm0219	Uni Illinois	0.224 (10)	0.239 (19)
16*	MICDIIR	N.A.	0.143 (15)	0.463 (1)
17	Roth et al.	Volume Graphics	0.070 (20)	0.300 (15)
18*	jkan	N.A.	0.218 (11)	0.250 (18)
19*	huni1115	N.A.	0.041 (25)	0.196 (22)
20*	mahendrakhened	IITM	0.117 (17)	0.348 (10)
21	Lipkova et al.	TU Munich	0.060 (22)	0.190 (23)
22*	jinqi	N.A.	0.044 (24)	0.232 (20)
23*	MIP_HQU	N.A.	0.030 (26)	0.220 (21)
24	Piraud et al.	TU Munich	0.068 (21)	0.325 (14)
25*	QiaoTian	N.A.	0.010 (27)	0.060 (25)

Table 7: Table MICCAI precision and recall scores for submissions. \* indicates missing short paper submission

moving closer to the performance of current interactive methods and the general requirements for clinical practice. This considerable improvement is best exemplified by the large performance increase of all methods between ISBI and MICCAI with even the best ISBI methods only performing better than the last 5 MICCAI methods and the second worst MICCAI method finishing 5th in the ISBI ranking. This can also be seen when looking at the rankings according to secondary metrics.

The considerable difference in both average and top global Dice and Dice per case scores indicate that small lesions are not captured very well and therefore artificially skew the global Dice values upwards. Rankings were considerably different according to the RVD metric since it only compares the lesion volume values of ground truth and method prediction but does not take positional information such as segmentation overlap into account.

In figure 8, segmentation results of sample images are shown. Both for ISBI (purple) and MICCAI (orange), next to the ground truth (green). The overall image indicates an improvement in the segmentation results of MICCAI compared to ISBI. For instance, the image at position 2x1 reveals a higher similarity of the MICCAI segmentation contour compared to the ground truth than ISBI. Also small tumor segmentations, e.g. in image position 1x1 bottom left and image position 1x3 bottom left, show a higher success rate at the MICCAI submissions. However, larger tumor lesions show no considerable improvements compared to ISBI submissions.

The reported segmentation results were almost exclusively achieved by fully automatic approaches and therefore come with their numerous benefits such as faster execution, lower cost and no inter- or intra operator variability. Hereby, we found that deep learning-based methods, specifically residual U-Nets, outperformed all other methods, which is in line with recent results of other medical image segmentation problems. Their capability of automatically learning the optimal features needed for segmentation as well as their layered structure allowing to recognize increasingly complex structural and textual pattern were key to delineating the liver lesions due to their highly variability in shape, location, size and texture. The resulting segmentations are robust against noise and preserve edges fairly well. They also obtained better scores than a novel state-of-the-art interactive method based on label propagation by Ma et al. and an unsupervised learning approach using Cahn-Hilliard Phase separation by Lipkov et al.

However, until fully automatic segmentation methods achieve a sufficiently high accuracy score for clinical use, interactive approaches remain the most important practical segmentation tool and therefore need further improvements. Generating the large labeled data sets that are currently necessary to train deep learning-based methods, is time-consuming and costly and might be more efficiently performed by more advanced semi-automatic methods thereby helping to bridge the gap to a final fully automatic solution. With a lesser reliance on extensive training and data sets, unsupervised methods rely on different features and inner workings and thereby not only help in obtaining valuable additional information about the lesion segmentation task but also enable the flexibility to apply the learnings to other data sets from different imaging modalities or physical structures.

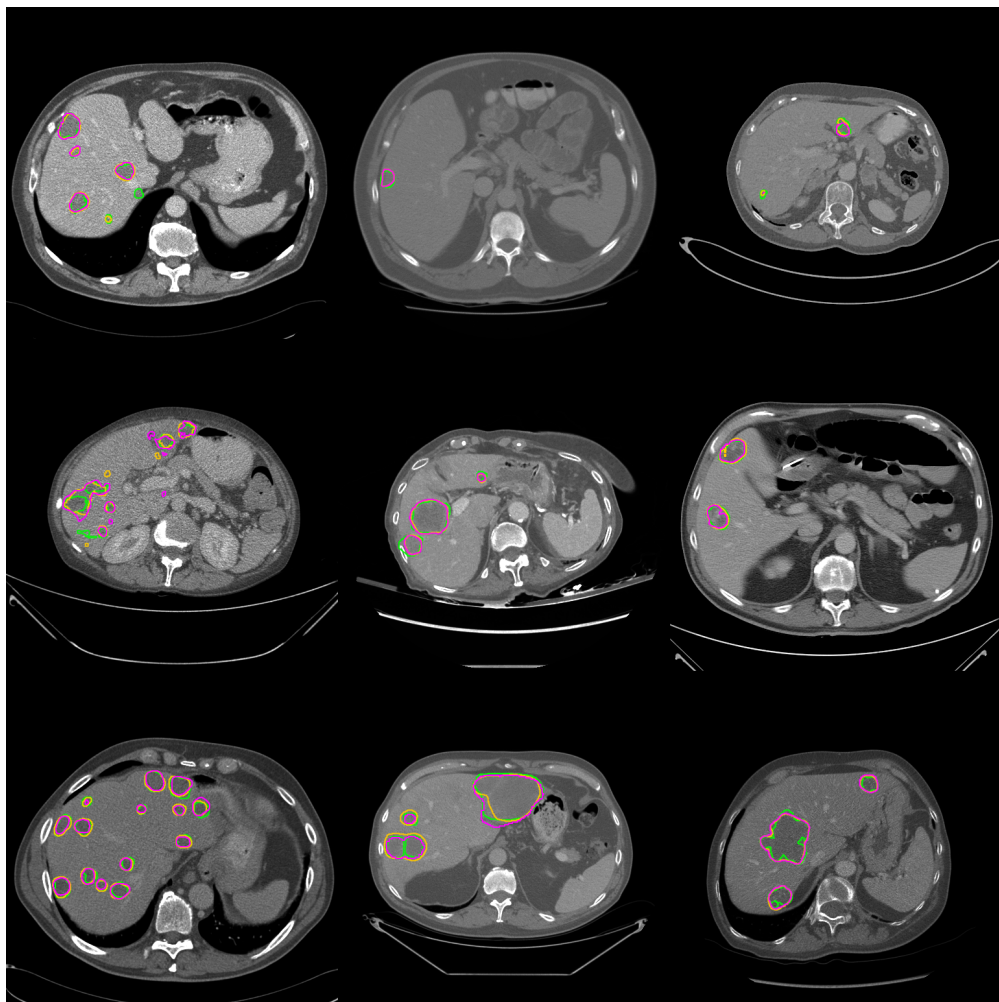


Figure 8: Segmentation results of the workshops MICCAI (orange) and ISBI (purple) compared to the ground truth (green). For each CT image, the best submitted segmentation from either workshop ranked by Dice per case was selected.

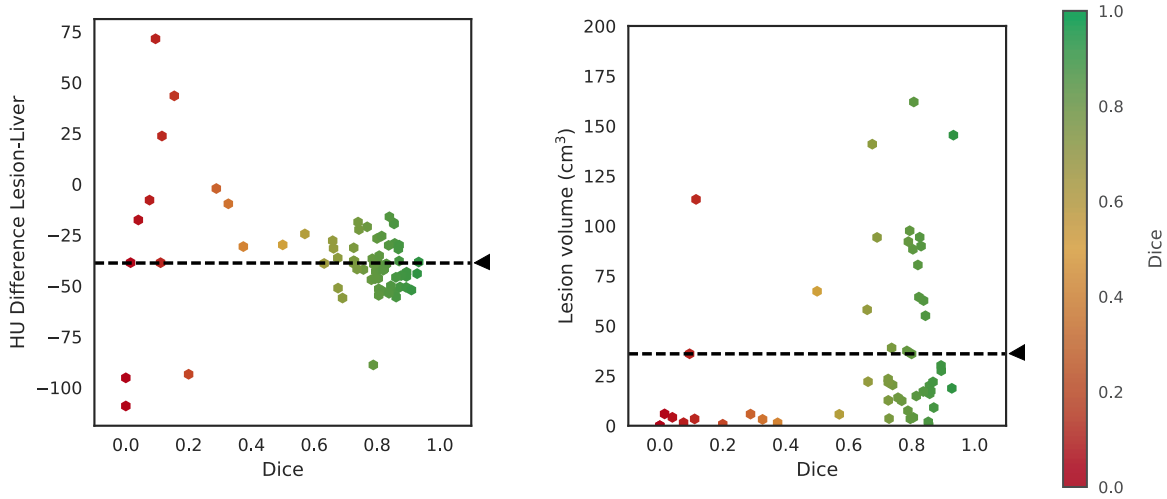


Figure 9: Analysis of lesion segmentation performance of MICCAI 2017 challenge best method.

However, as shown in figure 9, the submissions still lack precision for small tumor segmentation and high HU value differences. Overall, methods performed very well when segmenting large liver lesions but struggled more with smaller liver lesions (see Fig. 9). With many small lesions only having a diameter of a few voxels and the image resolution being a relatively high 512x512 even detecting such small structures is a difficult task due to the very small number of potentially differing surrounding pixels which would indicate a potential tumor border. This is exacerbated by the considerable noise and artifacts present in medical imaging which due to their size similarity, texture difference from the surrounding liver tissue and their arbitrary shape are difficult to distinguish from an actual liver lesion. Another important influence of the methods segmentation quality was the difference in lesion and liver HU values (see Fig. 9). Most methods performed best with this difference being in the range of -10 to -60. While it makes sense that an average difference in HU values eases the networks task of distinguishing liver and lesion tissue since a simple threshold-derived rule can be applied as part of the decision process, it is interesting that an even larger difference value did not result in an even better segmentation. A reason for this optimal performance of only a certain range of values might be the high concentration of individual slices in that range resulting in the network learning to judge these specific HU difference values as indicative of a lesion presence, but not higher ones due to too few data instances. The lower part of Fig.6 shows the combined influence of both lesion volume and liver-lesion-HU-value difference on lesion segmentation Dice score. One can see that the networks are much more susceptible to changes in HU-value difference than to changes in tumor size with many small tumors being segmented at a very Dice score but almost no lesions with too big of a HU-value difference achieving that same feat.

#### 4.7. *Winning algorithmic properties*

Overall, the best performing methods all relied on deep learning-based approaches in the form of cascaded U-Net derived architectures which are discussed further in the following subsections together with other commonly observed beneficial algorithm characteristics.

##### *U-Net-based architecture*

The U-Net architecture allows to obtain an output segmentation mask with the correct dimensionality, i.e. the same as the input ground truth segmentation mask, in one forward propagation of the network. This enables efficient end-to-end training and no necessity for additional resizing in post-processing thereby considerably simplifying architectural design and reducing the propensity for error. It also allows to generate segmentation masks at rapid speeds during testing and in the practical settings, which is one of the primary requirements for the usage of automatic segmentation methods in medical practice.

##### *Cascaded approach*

The common cascaded approaches allowed each network to focus and learn the relevant features for its specific task improving overall performance of both liver and tumor segmentation. In addition, network architecture design can be adapted to the specific network task resulting in a more effective and efficient training process and outcome. Also, earlier networks in the cascaded pipeline might help to standardize the intensity distribution for later networks which has been shown to improve overall performance.

##### *Residual connections*

The winning ISBI method by Han and many others also integrated residual connections in its architecture. Residual connections open a new channel of information flow through the network, giving later layers access to feature maps of previous layers and vice versa. It also improves gradient propagation resulting in faster convergence during training and higher overall network performance. While this is achieved by long skip connections between the downward and upward path of the network in case of the original U-Net, the residual architecture of this network also includes short skip residual connections around multiple layers alongside the downward or upward path. This provides the benefits of residual connections on a smaller scale, i.e. allowing the model to be more flexible and potentially use a coarse feature map representation instead of a finer output of multiple convolutional layers when needed. The second best ISBI method by Vorontsov also relied heavily on the idea of residual connections by organizing them in differently composed blocks, where multiple layers are combined with a short skip connection from the start of the block by adding it to the output feature map of all the block layers at the end of the block. MICCAIs second placed method by Li increased the number of residual connections even further by implementing a so-called DenseNet architecture consisting of dense blocks in which a feature map takes the outputs of all previous feature maps as an input via a residual connection giving another boost to the information flow through the network and mitigating the vanishing gradient problem.

### *Higher dimensionality*

Both the winning method at ISBI by Han, the best method at MICCAI by Zou and various other well performing approaches (e.g. Yuan) provided the network with stacks of image slices along the z-axis as input with the center slice being the slice to segmented. These extra input slices of this so called 2.5D architecture allow the model to benefit from additional contextual information of neighboring anatomic structures in the orthogonal direction thereby easing the task of identifying structural boundaries due to a wider choice of available potentially decisive features. While a complete 3D architecture might provide an even better performance, the influence of neighboring slices diminishes with increasing distance of these slices to the center slice to be segmented, resulting in the 2.5D architecture most likely capturing a considerable part of the advantages of a multidimensional design without suffering the current disadvantages of a full 3D set-up such as long training times and high resource requirements. However, Chlebus et al. used a small 3D network as the final network in a cascaded infrastructure to fuse the segmentation results of various previous networks into a final segmentation mask, while Li implemented a shallow 3D network to further refine the preliminary results of a first network. These good results not only prove the feasibility and usefulness of a 3D network architecture despite the currently limited memory availability when used as a supplementary role but also show their huge potential for future performance increase by being able to capture the whole volume context.

### *Ensemble learning*

The ensemble learning approach by Chlebus et al. trains 3 different U-Net derived networks on resampled axial, sagittal and coronal slices, respectively for liver segmentation and combines them via the aforementioned small 3D network. This allows each network to view lesions and learn distinguishing features along a different coordinate axis and then combine its individual knowledge with the other networks to yield a more holistic multi axes aware classifier. Bi et al. also employed a shape-invariant model fusion approach by providing multiple network with differently rescaled input data and then averaging the results. This allows to more easily detect formerly small lesions in its enlarged form by one network while simultaneous letting another network identify the exact image boundaries in images without additional resize-induced blurring. Vorontsov obtains the final segmentation mask by averaging over results from the four flip orientations as well as a slightly different model architecture. Yuan uses 5-fold cross validation combined with a bagging ensemble technique to fuse the results of 6 individual models. Zou as MICCAI's winning method relies heavily on ensemble learning using it in both the liver segmentation and the tumor segmentation step as the first part and second part of a cascaded approach. Each of these two parts are further divided into two subparts, one of which using 2D slice-wise and the other 2.5D stack-wise inputs to train multiple networks each. These networks are each implemented with different architecture such as a varying depth, width, number of feature maps or the existence of additional drop-out layers and combine to form one segmentation mask via intersections. The two intersection masks of the slice-input networks and the stack-input networks are the fused via a union operation to generate the final liver or tumor segmentation mask of the cascaded pipeline. This multi-layered ensemble techniques not only allows to detect a large

number of different features due to the sheer number of different networks but also applies them at varying levels of granularity along the segmentation pipeline while simultaneously increasing its flexibility by employing different fusion techniques.

#### *Loss function*

Weighted cross entropy is used by many winning methods (e.g. Han, Zou, Li) as a loss function to mitigate the negative effects of high class imbalance present in the LiTS dataset. In addition, Li applies so called hard pixel mining learning and only uses the 10% of voxels with the highest misclassification rate in his loss calculations to force the network to focus on minimizing the error of the up until that point most difficult voxels. Other common loss functions among the best performing methods were Dice loss (e.g. Vorontsov et al) and Jaccard loss (e.g. Yuan), which are both derived from the respective overlap metrics by inverting or subtracting the Dice or Jaccard score from 1 to obtain a quantity to be minimized. This allows the network to directly optimize its parameters according to the actual final evaluation metric instead of indirectly via cross entropy and thereby also implicitly incorporate class imbalance in its learning process without the explicit introduction of class specific weights other class re-balancing techniques. The Jaccard loss has the additional benefit that its corresponding metric fulfills the triangle inequality and is therefore considered a true distance metric.

#### *Activation function*

Han’s winning ISBI method applied PReLU activation instead of the more common ReLU allowing the network to also learn the optimal leakage coefficient of the activation function.

#### *Pre-processing*

The most common pre-processing technique used by almost all methods was HU-value clipping to only consider a range of relevant liver-related values. This generally improves performance by allowing the network to focus on the important image aspects for the segmentation task but comes at the cost of decreased flexibility of applying the methods to other data sets. Also, there was no clear consensus but rather significant variation of the optimal clipping boundary HU values indicating potentially suboptimal value choices by some methods. Another frequently used technique was data normalization which simplifies the networks learning task by providing more easily comparable images as input. Furthermore, Zou filtered out very small lesions as noise before training to prevent the network from learning non-realistic tumor structures and potentially produce many false positives. Chlebus et al. specifically mentioned to train the networks with original resolution input images thereby allowing for all image detail to be made available to the network and not being lost in potential resizing operation. Han resampled input images for liver segmentation to a fixed resolution of 1x1x2.5mm since the liver region is not as susceptible to resizing-induced blurring as lesions due to its size and the network can therefore profit from the easier comparability of inputs due to their homogeneous resolution.

### *Data augmentation*

Most methods made use of various data augmentation techniques to combat overfitting caused by the small data set size and increase the robustness of the method. Hereby, the standard geometric transformations such as shifting, flipping, rotating, scaling or cropping were the most frequently applied and showed a positive effect on the final performance. Vorontsov et al. and in part Yuan implemented elastic deformation as a data augmentation strategy providing an effective way to realistically increase data set size. Yuan also applied a random contrast normalization to each images input channels.

### *Post-processing*

Almost all methods utilize connected component labeling as a post-processing step. Another very common technique was to remove or cut off lesions not fully contained within the liver boundaries. The overall best method by Zou applies various other post-processing techniques. They propose a custom criteria of removing lesions as noise if they have relatively large size in one slice but simultaneously a very small size in an adjacent slice. Next, they observe that lesion size will increase for each slice starting from the first lesion containing slice until the maximum lesion size slice and then decrease in a similar way until no lesion remains. Based on this they implement a custom lesion hole filling algorithm that relies on the lesion volumes of adjacent slices. Furthermore, they tackle the previously mentioned bad performance in small lesion detection by implementing a special residual network with small lesion containing patches as input and remove lesions with less than 40% overlap. All three techniques effectively mitigate one of the main observed problems of noisy data, incorrect holes in lesion segmentations and difficulty in small lesion segmentation and therefore considerably contribute to the methods success. Other commonly used approaches to fill erroneous holes in lesion segmentations employed morphological filtering (e.g. Bi). Another observed issue of many methods was a relatively high number of false positives, which Chlebus tackled by filtering them out with a Random Forest classifier. Han applied a custom criteria to this issue by calculating the maximal lesion probability value of a connected lesion component and removing the lesion if this value is below an empirically determined threshold of 0.8.

## **5. Discussions**

### *5.1. Lessons learned and future work*

Experience from organizing LiTS two times has taught us lessons relevant for future medical segmentation benchmark challenges and their organizers. Given that many of the algorithms that participated in his study offered good liver segmentation results compared to liver, it seems valuable to label evaluate liver tumors based on their different characteristics in terms of size and type. Since almost all submitted methods are based on deep learning architectures, the number of 131 training instances should be increased to avoid segmentation performance limits. To mitigate this issue, the costly and time-consuming

data acquisition process could be made more efficient by using better and improved semi-automatic segmentation techniques. This can be seen as an indicator to split future LiTS challenges in order to attract submissions for more semi-automatic methods.

Further, we recommended to provide multiple ground truth segmentation. However modern methods e.g. Deep Convolutional Neural Networks are able to overcome operator dependent annotation or errors in the training data that are present when only a single rater labels each case. Comparing results of LiTS's to previous liver (and tumor) challenges it is advised to provide larger training data sets because state-of-the-art methods highly benefit from larger training datasets.

Moreover, we suggest that future organizers consider the desired outcome before offering normalized and preprocessed data. The advantage of offering a normalized dataset with standardized resolution and homogenized gray-level distributions or even crops helps to compare the trained models provided by participants. Furthermore, it supports potential participants to overcome initial difficulties and can lead to more contributions. However, the trend towards deep learning methods increases the importance of data preprocessing. If preprocessing methods are relevant, we advice to offer the original data in a standardized data format s.a. Nifti and provide interface instructions for common programming languages s.a. Python, R and Matlab.

## 5.2. *Caveats*

While general architectural characteristics of the winnings models can be derived, it remains difficult to provide recommendations with regards to the exact network design. For example, the number and order of different layers such as convolutional, activation, drop-out or batch normalization layers or the position of residual connections are mostly guided by rough ideas instead of strict, proven guidelines. Other architectural features such as kernel size or hyperparameters such as batch size and learning rate are mostly narrowed down to a specific range but then arbitrarily chosen within this interval. Ample exploration of such characteristics is hindered by long training times making trial runs costly. This also applies to the choice of weights in the cross entropy function, which are mostly empirically set after only a few trial runs. The sparse use of 3D architectures showed promising results in this challenge but is currently not implementable on a larger scale due to memory constraints. While ensemble learning techniques generally outperformed individual methods, both training and test time are increased significantly with the former further delaying research trial progress and the latter complicating eventual clinical usage. Therefore, the limited available memory also sets a constraint to the degree and size of model fusion usage. Similar issues hinder the other beneficial integration of more residual connections or a higher depth of U-net based models.

While large tumors were segmented very well, the methods were not able to achieve sufficiently high Dice scores for smaller lesions. The problem was recognized by some methods in the challenge and corresponding countermeasures in loss functions and post-processing steps were developed but further research is still needed to improve small lesion detection performance to the clinically required level of accuracy.

## 6. Summary and Conclusion

In this paper we presented the LiTS liver tumor segmentation benchmark. We generated the largest public dataset available for liver and liver tumor segmentation tasks evaluated, analyzed and ranked a high number of state-of-the-art medical image segmentation methods. While liver tumor segmentation is difficult, currently available algorithms can reach Dice scores of over 95% for liver segmentation and over 70% for liver tumor segmentation. For analyzed methods, segmenting small liver tumor regions automatically still remain as a difficult task. This suggests that, in addition to focus further on heterogeneous liver tumor structures, future improvements can be achieved by investigating on methods focusing on very local image structures.

## References

- [1] T. Heimann, B. Van Ginneken, M. Styner, Y. Arzhaeva, V. Aurich, C. Bauer, A. Beck, C. Becker, R. Beichel, G. Bekes, F. Bello, G. Binnig, H. Bischof, A. Bornik, P. Cashman, Y. Chi, A. Crdova, B. Dawant, M. Fidrich, J. Furst, D. Furukawa, L. Grenacher, J. Hornegger, D. Kainmller, R. Kitney, H. Kobatake, H. Lamecker, T. Lange, J. Lee, B. Lennon, R. Li, S. Li, H. Meinzer, G. Nmeth, D. Raicu, A. Rau, E. Van Rikxoort, M. Rousson, L. Rusk, K. Saddi, G. Schmidt, D. Seghers, A. Shimizu, P. Slagmolen, E. Sorantin, G. Soza, R. Susomboon, J. Waite, A. Wimmer, I. Wolf, Comparison and evaluation of methods for liver segmentation from ct datasets, *IEEE Transactions on Medical Imaging* 28 (8) (2009) 1251–1265. doi:10.1109/TMI.2009.2013851.
- [2] P. F. Christ, M. E. A. Elshaer, F. Ettlinger, S. Tatavarty, M. Bickel, P. Bilic, M. Rempfler, M. Armbruster, F. Hofmann, M. D'Anastasi, W. H. Sommer, S.-A. Ahmadi, B. H. Menze, Automatic Liver and Lesion Segmentation in CT Using Cascaded Fully Convolutional Neural Networks and 3D Conditional Random Fields, *MICCAI*, 2016, pp. 415–423.
- [3] E. Eisenhauer, P. Therasse, J. Bogaerts, L. Schwartz, D. Sargent, R. Ford, J. Dancey, S. Arbuck, S. Gwyther, M. Mooney, et al., New response evaluation criteria in solid tumours: revised recist guideline (version 1.1), *European journal of cancer* 45 (2) (2009) 228–247.
- [4] B. W. Stewart, C. P. Wild, *World cancer report 2014*, Tech. rep., WHO Press, World Health Organization (2014). arXiv:1011.1669, doi:9283204298.  
URL <http://www.videnza.org/wp-content/uploads/World-Cancer-Report-2014.pdf>
- [5] L. E. Hann, C. B. Winston, K. T. Brown, T. Akhurst, Diagnostic imaging approaches and relationship to hepatobiliary cancer staging and therapy, in: *Seminars in surgical oncology*, Vol. 19, Wiley Online Library, 2000, pp. 94–115.
- [6] S. Rossi, M. Di Stasi, E. Buscarini, P. Quaretti, F. Garbagnati, L. Squassante, C. Paties, D. Silverman, L. Buscarini, Percutaneous rf interstitial thermal ablation in the treatment of hepatic cancer., *AJR. American journal of roentgenology* 167 (3) (1996) 759–768.
- [7] T. Livraghi, A. Giorgio, G. Marin, A. Salmi, I. De Sio, L. Bolondi, M. Pompili, F. Brunello, S. Lazzaroni, G. Torzilli, Hepatocellular carcinoma and cirrhosis in 746 patients: long-term results of percutaneous ethanol injection., *Radiology* 197 (1) (1995) 101–108.
- [8] K. S. Albain, R. S. Swann, V. W. Rusch, A. T. Turrissi, F. A. Shepherd, C. Smith, Y. Chen, R. B. Livingston, R. H. Feins, D. R. Gandara, et al., Radiotherapy plus chemotherapy with or without surgical resection for stage iii non-small-cell lung cancer: a phase iii randomised controlled trial, *The Lancet* 374 (9687) (2009) 379–386.
- [9] R. Yamada, M. Sato, M. Kawabata, H. Nakatsuka, K. Nakamura, S. Takashima, Hepatic artery embolization in 120 patients with unresectable hepatoma., *Radiology* 148 (2) (1983) 397–401.
- [10] J. Chapiro, R. Duran, M. Lin, R. E. Schernthaler, Z. Wang, B. Gorodetski, J.-F. Geschwind, Identifying staging markers for hepatocellular carcinoma before transarterial chemoembolization: comparison of three-dimensional quantitative versus non–three-dimensional imaging markers, *Radiology* 275 (2) (2014) 438–447.
- [11] E. Eisenhauer, P. Therasse, J. Bogaerts, L. Schwartz, D. Sargent, R. Ford, J. Dancey, S. Arbuck, S. Gwyther, M. Mooney, et al., 32 invited new response evaluation criteria in solid tumors: revised recist guideline version 1.1, *European Journal of Cancer Supplements* 6 (12) (2008) 13.
- [12] M. Moghbel, S. Mashohor, R. Mahmud, M. I. B. Saripan, Review of liver segmentation and computer assisted detection/diagnosis methods in computed tomography, *Artif. Intell. Rev.* (2017) 1–41doi:10.1007/s10462-017-9550-x.
- [13] B. Nordlinger, M. Guiguet, J.-C. Vaillant, P. Balladur, K. Boudjema, P. Bachellier, D. Jaeck, Surgical resection of colorectal carcinoma metastases to the liver: a prognostic scoring system to improve case selection, based on 1568 patients, *Cancer: Interdisciplinary International Journal of the American Cancer Society* 77 (7) (1996) 1254–1262.
- [14] S. Jagannath, W. S. Velasquez, S. L. Tucker, L. M. Fuller, P. W. McLaughlin, J. T. Manning, L. B. North, F. C. Cabanillas, Tumor burden assessment and its implication for a prognostic model in advanced diffuse large-cell lymphoma., *Journal of Clinical Oncology* 4 (6) (1986) 859–865.

[15] M. Blachier, H. Leleu, M. Peck-Radosavljevic, D.-C. Valla, F. Roudot-Thoraval, The burden of liver disease in europe: a review of available epidemiological data, *Journal of hepatology* 58 (3) (2013) 593–608.

[16] P. G. Gobbi, C. Broglia, G. Di Giulio, M. Mantelli, P. Anselmo, F. Merli, P. L. Zinzani, G. Rossi, V. Callea, E. Iannitto, et al., The clinical value of tumor burden at diagnosis in hodgkin lymphoma, *Cancer: Interdisciplinary International Journal of the American Cancer Society* 101 (8) (2004) 1824–1834.

[17] L. Bornemann, V. Dicken, J.-M. Kuhnigk, D. Wormanns, H.-O. Shin, H.-C. Bauknecht, V. Diehl, M. Fabel, S. Meier, O. Kress, et al., Oncotreat: a software assistant for cancer therapy monitoring, *International Journal of Computer Assisted Radiology and Surgery* 1 (5) (2007) 231–242.

[18] C. P. Heussel, S. Meier, S. Wittelsberger, H. Götte, P. Mildenberger, H.-U. Kauczor, Follow-up ct measurement of liver malignoma according to recist and who vs. volumetry, *RoFo: Fortschritte auf dem Gebiete der Rontgenstrahlen und der Nuklearmedizin* 179 (9) (2007) 958–964.

[19] J.-M. Kuhnigk, V. Dicken, L. Bornemann, A. Bakai, D. Wormanns, S. Krass, H.-O. Peitgen, Morphological segmentation and partial volume analysis for volumetry of solid pulmonary lesions in thoracic ct scans, *IEEE Transactions on Medical Imaging* 25 (4) (2006) 417–434.

[20] M. Puesken, B. Buerke, J. Gerss, B. Frisch, F. Beyer, M. Weckesser, H. Seifarth, W. Heindel, J. Wessling, Prediction of lymph node manifestations in malignant lymphoma: significant role of volumetric compared with established metric lymph node analysis in multislice computed tomography, *Journal of computer assisted tomography* 34 (4) (2010) 564–569.

[21] H.-C. Bauknecht, V. C. Romano, P. Rogalla, R. Klingebiel, C. Wolf, L. Bornemann, B. Hamm, P. A. Hein, Intra-and interobserver variability of linear and volumetric measurements of brain metastases using contrast-enhanced magnetic resonance imaging, *Investigative radiology* 45 (1) (2010) 49–56.

[22] T. F. Cootes, C. J. Taylor, D. H. Cooper, J. Graham, Active shape models-their training and application, *Computer vision and image understanding* 61 (1) (1995) 38–59.

[23] T. Heimann, I. Wolf, H.-P. Meinzer, Active shape models for a fully automated 3d segmentation of the liver—an evaluation on clinical data, *Medical Image Computing and Computer-Assisted Intervention–MICCAI 2006* (2006) 41–48.

[24] T. Heimann, S. Münzing, H.-P. Meinzer, I. Wolf, A shape-guided deformable model with evolutionary algorithm initialization for 3d soft tissue segmentation, in: *Information Processing in Medical Imaging*, Springer, 2007, pp. 1–12.

[25] D. Kainmüller, T. Lange, H. Lamecker, Shape constrained automatic segmentation of the liver based on a heuristic intensity model, in: *Proc. MICCAI Workshop 3D Segmentation in the Clinic: A Grand Challenge*, 2007, pp. 109–116.

[26] X. Zhang, J. Tian, K. Deng, Y. Wu, X. Li, Automatic liver segmentation using a statistical shape model with optimal surface detection, *IEEE Transactions on Biomedical Engineering* 57 (10) (2010) 2622–2626.

[27] S. Tomoshige, E. Oost, A. Shimizu, H. Watanabe, S. Nawano, A conditional statistical shape model with integrated error estimation of the conditions; application to liver segmentation in non-contrast ct images, *Medical image analysis* 18 (1) (2014) 130–143.

[28] X. Wang, J. Yang, D. Ai, Y. Zheng, S. Tang, Y. Wang, Adaptive mesh expansion model (amem) for liver segmentation from ct image, *PloS one* 10 (3) (2015) e0118064.

[29] H. Lamecker, T. Lange, M. Seebass, Segmentation of the liver using a 3D statistical shape model, Konrad-Zuse-Zentrum für Informationstechnik Berlin, 2004.

[30] K. A. Saddi, M. Rousson, C. Chefdhotel, F. Cheriet, Global-to-local shape matching for liver segmentation in ct imaging, in: *Proceedings of MICCAI workshop on 3D segmentation in the clinic: a grand challenge*, 2007, pp. 207–214.

[31] H. Ling, S. K. Zhou, Y. Zheng, B. Georgescu, M. Suehling, D. Comaniciu, Hierarchical, learning-based automatic liver segmentation, in: *Computer Vision and Pattern Recognition, 2008. CVPR 2008. IEEE Conference on*, IEEE, 2008, pp. 1–8.

[32] H. Park, P. H. Bland, C. R. Meyer, Construction of an abdominal probabilistic atlas and its application

in segmentation, *IEEE Transactions on medical imaging* 22 (4) (2003) 483–492.

[33] X. Zhou, T. Kitagawa, T. Hara, H. Fujita, X. Zhang, R. Yokoyama, H. Kondo, M. Kanematsu, H. Hoshi, Constructing a probabilistic model for automated liver region segmentation using non-contrast x-ray torso ct images, *Medical Image Computing and Computer-Assisted Intervention-MICCAI 2006* (2006) 856–863.

[34] P. Slagmolen, A. Elen, D. Seghers, D. Loeckx, F. Maes, K. Haustermans, Atlas based liver segmentation using nonrigid registration with a b-spline transformation model, in: *Proceedings of MICCAI workshop on 3D segmentation in the clinic: a grand challenge*, 2007, pp. 197–206.

[35] Z. Xu, R. P. Burke, C. P. Lee, R. B. Baucom, B. K. Poulose, R. G. Abramson, B. A. Landman, Efficient multi-atlas abdominal segmentation on clinically acquired ct with simple context learning, *Medical image analysis* 24 (1) (2015) 18–27.

[36] E. van Rikxoort, Y. Arzhaeva, B. van Ginneken, Automatic segmentation of the liver in computed tomography scans with voxel classification and atlas matching, in: *Proceedings of the MICCAI Workshop*, Citeseer, 2007, pp. 101–108.

[37] T. Okada, R. Shimada, M. Hori, M. Nakamoto, Y.-W. Chen, H. Nakamura, Y. Sato, Automated segmentation of the liver from 3d ct images using probabilistic atlas and multilevel statistical shape model, *Academic radiology* 15 (11) (2008) 1390–1403.

[38] S.-J. Lim, Y.-Y. Jeong, C.-W. Lee, Y.-S. Ho, Automatic segmentation of the liver in ct images using the watershed algorithm based on morphological filtering, in: *Proc. of SPIE Vol, Vol. 5370*, 2004, p. 1659.

[39] S.-J. Lim, Y.-Y. Jeong, Y.-S. Ho, Automatic liver segmentation for volume measurement in ct images, *Journal of Visual Communication and Image Representation* 17 (4) (2006) 860–875.

[40] S.-J. Lim, Y.-Y. Jeong, Y.-S. Ho, Segmentation of the liver using the deformable contour method on ct images, *Advances in Multimedia Information Processing-PCM 2005* (2005) 570–581.

[41] L. Massoptier, S. Casciaro, Fully automatic liver segmentation through graph-cut technique, in: *Engineering in Medicine and Biology Society, 2007. EMBS 2007. 29th Annual International Conference of the IEEE*, IEEE, 2007, pp. 5243–5246.

[42] W. Wu, Z. Zhou, S. Wu, Y. Zhang, Automatic liver segmentation on volumetric ct images using supervoxel-based graph cuts, *Computational and mathematical methods in medicine* 2016.

[43] A. Shimizu, K. Nakagomi, T. Narihira, H. Kobatake, S. Nawano, K. Shinozaki, K. Ishizu, K. Togashi, Automated segmentation of 3d ct images based on statistical atlas and graph cuts, in: *International MICCAI Workshop on Medical Computer Vision*, Springer, 2010, pp. 214–223.

[44] L. Gao, D. G. Heath, B. S. Kuszyk, E. K. Fishman, Automatic liver segmentation technique for three-dimensional visualization of ct data., *Radiology* 201 (2) (1996) 359–364.

[45] A. M. Anter, A. E. Hassanien, M. A. A. ElSoud, M. F. Tolba, Neutrosophic sets and fuzzy c-means clustering for improving ct liver image segmentation, in: *Proceedings of the Fifth International Conference on Innovations in Bio-Inspired Computing and Applications IBICA 2014*, Springer, 2014, pp. 193–203.

[46] A. Mostafa, A. Fouad, M. A. Elfattah, A. E. Hassanien, H. Hefny, S. Y. Zhu, G. Schaefer, Ct liver segmentation using artificial bee colony optimisation, *Procedia Computer Science* 60 (2015) 1622–1630.

[47] M. Moghbel, S. Mashohor, R. Mahmud, M. I. B. Saripan, Automatic liver segmentation on computed tomography using random walkers for treatment planning, *EXCLI journal* 15 (2016) 500.

[48] C. Huang, X. Li, F. Jia, Automatic liver segmentation using multiple prior knowledge models and free-form deformation, in: *Proceedings of the VISCERAL organ segmentation and landmark detection benchmark at the 2014 IEEE international symposium on biomedical imaging (ISBI)*, 2014.

[49] X. Li, C. Huang, F. Jia, Z. Li, C. Fang, Y. Fan, Automatic liver segmentation using statistical prior models and free-form deformation, in: *International MICCAI Workshop on Medical Computer Vision*, Springer, 2014, pp. 181–188.

[50] Y. Zheng, D. Ai, P. Zhang, Y. Gao, L. Xia, S. Du, X. Sang, J. Yang, Feature learning based random walk for liver segmentation, *PloS one* 11 (11) (2016) e0164098.

[51] D.-Y. Tsai, N. Tanahashi, Neural-network-based boundary detection of liver structure in ct images for

3-d visualization, in: Neural Networks, 1994. IEEE World Congress on Computational Intelligence., 1994 IEEE International Conference on, Vol. 6, IEEE, 1994, pp. 3484–3489.

[52] G. Litjens, T. Kooi, B. E. Bejnordi, A. A. A. Setio, F. Ciompi, M. Ghafoorian, J. A. van der Laak, B. van Ginneken, C. I. Sánchez, A survey on deep learning in medical image analysis, arXiv preprint arXiv:1702.05747.

[53] O. Ronneberger, P. Fischer, T. Brox, U-net: Convolutional networks for biomedical image segmentation, in: MICCAI, Vol. 9351, 2015, pp. 234–241.

[54] J. Long, E. Shelhamer, T. Darrell, Fully convolutional networks for semantic segmentation, CVPR.

[55] H. Noh, S. Hong, B. Han, Learning deconvolution network for semantic segmentation, in: Proceedings of the IEEE International Conference on Computer Vision, 2015, pp. 1520–1528.

[56] A. Ben-Cohen, I. Diamant, E. Klang, M. Amitai, H. Greenspan, Fully convolutional network for liver segmentation and lesions detection, in: International Workshop on Large-Scale Annotation of Biomedical Data and Expert Label Synthesis, Springer, 2016, pp. 77–85.

[57] F. Lu, F. Wu, P. Hu, Z. Peng, D. Kong, Automatic 3d liver location and segmentation via convolutional neural network and graph cut, International journal of computer assisted radiology and surgery 12 (2) (2017) 171–182.

[58] Q. Dou, H. Chen, Y. Jin, L. Yu, J. Qin, P.-A. Heng, 3d deeply supervised network for automatic liver segmentation from ct volumes, in: International Conference on Medical Image Computing and Computer-Assisted Intervention, Springer, 2016, pp. 149–157.

[59] P. Hu, F. Wu, J. Peng, P. Liang, D. Kong, Automatic 3d liver segmentation based on deep learning and globally optimized surface evolution, Physics in medicine and biology 61 (24) (2016) 8676.

[60] L. Rusko, G. Bekes, G. Nemeth, M. Fidrich, Fully automatic liver segmentation for contrast-enhanced ct images, MICCAI Wshp. 3D Segmentation in the Clinic: A Grand Challenge 2 (7).

[61] R. Susomboon, D. S. Raicu, J. Furst, A hybrid approach for liver segmentation, in: Proceedings of MICCAI workshop on 3D segmentation in the clinic: a grand challenge, 2007, pp. 151–160.

[62] A. Beck, V. Aurich, Hepatux-a semiautomatic liver segmentation system, 3D Segmentation in The Clinic: A Grand Challenge (2007) 225–233.

[63] Y. Boykov, O. Veksler, R. Zabih, Fast approximate energy minimization via graph cuts, IEEE Transactions on pattern analysis and machine intelligence 23 (11) (2001) 1222–1239.

[64] R. Beichel, T. Pock, C. Janko, R. B. Zotter, B. Reitinger, A. Bornik, K. Palagyi, E. Sorantin, G. Werksgartner, H. Bischof, et al., Liver segment approximation in ct data for surgical resection planning, in: Proceedings of SPIE, Vol. 5370, 2004, pp. 1435–1446.

[65] C. Florin, N. Paragios, G. Funka-Lea, J. Williams, Liver segmentation using sparse 3d prior models with optimal data support, in: Information Processing in Medical Imaging, Springer, 2007, pp. 38–49.

[66] G. Chartrand, T. Cresson, R. Chav, A. Gotra, A. Tang, J. DeGuise, Semi-automated liver ct segmentation using laplacian meshes, in: Biomedical Imaging (ISBI), 2014 IEEE 11th International Symposium on, IEEE, 2014, pp. 641–644.

[67] A. Schenk, G. Prause, H.-O. Peitgen, Efficient semiautomatic segmentation of 3d objects in medical images, in: MICCAI, Vol. 1935, Springer, 2000, pp. 186–195.

[68] M. Goryawala, S. Gulec, R. Bhatt, A. J. McGoron, M. Adjouadi, A low-interaction automatic 3d liver segmentation method using computed tomography for selective internal radiation therapy, BioMed research international 2014.

[69] L. Fernández-de Manuel, J. L. Rubio, M. J. Ledesma-Carbayo, J. Pascau, J. M. Tellado, E. Ramón, M. Desco, A. Santos, 3d liver segmentation in preoperative ct images using a levelsets active surface method, in: Engineering in Medicine and Biology Society, 2009. EMBC 2009. Annual International Conference of the IEEE, IEEE, 2009, pp. 3625–3628.

[70] L. Soler, H. Delingette, G. Malandain, J. Montagnat, N. Ayache, C. Koehl, O. Dourthe, B. Malassagne, M. Smith, D. Mutter, et al., Fully automatic anatomical, pathological, and functional segmentation from ct scans for hepatic surgery, Computer Aided Surgery 6 (3) (2001) 131–142.

[71] M. Ciecholowski, M. R. Ogiela, Automatic segmentation of single and multiple neoplastic hepatic lesions in ct images, in: International Work-Conference on the Interplay Between Natural and Artificial

Computation, Springer, 2007, pp. 63–71.

[72] H. A. Nugroho, D. Ihtatho, H. Nugroho, Contrast enhancement for liver tumor identification, in: MICCAI workshop, Vol. 41, 2008, p. 201.

[73] N. H. Abdel-massieh, M. M. Hadhoud, K. M. Amin, Fully automatic liver tumor segmentation from abdominal ct scans, in: Computer Engineering and Systems (ICCES), 2010 International Conference on, IEEE, 2010, pp. 197–202.

[74] J. H. Moltz, L. Bornemann, V. Dicken, H. Peitgen, Segmentation of liver metastases in ct scans by adaptive thresholding and morphological processing, in: MICCAI workshop, Vol. 41, 2008, p. 195.

[75] J. H. Moltz, L. Bornemann, J.-M. Kuhnigk, V. Dicken, E. Peitgen, S. Meier, H. Bolte, M. Fabel, H.-C. Bauknecht, M. Hittinger, et al., Advanced segmentation techniques for lung nodules, liver metastases, and enlarged lymph nodes in ct scans, *IEEE Journal of selected topics in signal processing* 3 (1) (2009) 122–134.

[76] M. Kass, A. Witkin, D. Terzopoulos, Snakes: Active contour models, *International journal of computer vision* 1 (4) (1988) 321–331.

[77] I. Ben-Dan, E. Shenhav, Liver tumor segmentation in ct images using probabilistic methods, in: MICCAI Workshop, Vol. 41, 2008, p. 43.

[78] M. G. Linguraru, W. J. Richbourg, J. Liu, J. M. Watt, V. Pamulapati, S. Wang, R. M. Summers, Tumor burden analysis on computed tomography by automated liver and tumor segmentation, *Medical Imaging, IEEE Transactions on* 31 (10) (2012) 1965–1976.

[79] S. Osher, J. A. Sethian, Fronts propagating with curvature-dependent speed: algorithms based on hamilton-jacobi formulations, *Journal of computational physics* 79 (1) (1988) 12–49.

[80] D. Smeets, B. Stijnen, D. Loeckx, B. De Dobbelaer, P. Suetens, Segmentation of liver metastases using a level set method with spiral-scanning technique and supervised fuzzy pixel classification, in: MICCAI workshop, Vol. 42, 2008, p. 43.

[81] D. Jiménez Carretero, L. Fernández de Manuel, J. Pascau González Garzón, J. M. Tellado, E. Ramon, M. Desco Menéndez, A. Santos, M. J. Ledesma Carbayo, Optimal multiresolution 3d level-set method for liver segmentation incorporating local curvature constraints.

[82] A. Hoogi, A. Subramaniam, R. Veerapaneni, D. L. Rubin, Adaptive estimation of active contour parameters using convolutional neural networks and texture analysis, *IEEE transactions on medical imaging* 36 (3) (2017) 781–791.

[83] L. Massoptier, S. Casciaro, A new fully automatic and robust algorithm for fast segmentation of liver tissue and tumors from ct scans, *European radiology* 18 (8) (2008) 1658.

[84] Y. Häme, Liver tumor segmentation using implicit surface evolution, *The Midas Journal* (2008) 1–10.

[85] E. Vorontsov, N. Abi-Jaoudeh, S. Kadoury, Metastatic liver tumor segmentation using texture-based omni-directional deformable surface models, in: International MICCAI Workshop on Computational and Clinical Challenges in Abdominal Imaging, Springer, 2014, pp. 74–83.

[86] A. Shimizu, T. Narihira, D. Furukawa, H. Kobatake, S. Nawano, K. Shinozaki, Ensemble segmentation using adaboost with application to liver lesion extraction from a ct volume, in: Proc. MICCAI Workshop on 3D Segmentation in the Clinic: A Grand Challenge II., NY, USA, 2008.

[87] Y. Li, S. Hara, K. Shimura, A machine learning approach for locating boundaries of liver tumors in ct images, in: null, IEEE, 2006, pp. 400–403.

[88] J. Wen, X. Zhang, Y. Xu, Z. Li, L. Liu, Comparison of adaboost and logistic regression for detecting colorectal cancer patients with synchronous liver metastasis, in: Biomedical and Pharmaceutical Engineering, 2009. ICBPE'09. International Conference on, IEEE, 2009, pp. 1–6.

[89] P.-H. Conze, V. Noblet, F. Rousseau, F. Heitz, V. De Blasi, R. Memeo, P. Pessaux, Scale-adaptive supervoxel-based random forests for liver tumor segmentation in dynamic contrast-enhanced ct scans, *International journal of computer assisted radiology and surgery* 12 (2) (2017) 223–233.

[90] F. Lu, F. Wu, P. Hu, Z. Peng, D. Kong, Automatic 3d liver location and segmentation via convolutional neural network and graph cut, *International Journal of Computer Assisted Radiology and Surgery* 12 (2) (2017) 171–182. doi:10.1007/s11548-016-1467-3.

URL <https://doi.org/10.1007/s11548-016-1467-3>

[91] J. Stawiaski, E. Decenciere, F. Bidault, Interactive liver tumor segmentation using graph-cuts and watershed, in: Workshop on 3D Segmentation in the Clinic: A Grand Challenge II. Liver Tumor Segmentation Challenge. MICCAI, New York, USA, 2008.

[92] A. Choudhary, N. Moretto, F. P. Ferrarese, G. A. Zamboni, An entropy based multi-thresholding method for semi-automatic segmentation of liver tumors, in: MICCAI workshop, Vol. 41, 2008, pp. 43–49.

[93] Y. Taieb, O. Eliassaf, M. Freiman, L. Joskowicz, J. Sosna, An iterative bayesian approach for liver analysis: tumors validation study, in: MICCAI workshop, Vol. 41, 2008, p. 43.

[94] W. Huang, Y. Yang, Z. Lin, G.-B. Huang, J. Zhou, Y. Duan, W. Xiong, Random feature subspace ensemble based extreme learning machine for liver tumor detection and segmentation, in: Engineering in Medicine and Biology Society (EMBC), 2014 36th Annual International Conference of the IEEE, IEEE, 2014, pp. 4675–4678.

[95] J. Zhou, W. Xiong, Q. Tian, Y. Qi, J. Liu, W. K. Leow, T. Han, S. K. Venkatesh, S.-c. Wang, Semi-automatic segmentation of 3d liver tumors from ct scans using voxel classification and propagational learning, in: MICCAI workshop, Vol. 41, 2008, p. 43.

[96] X. Zhang, J. Tian, D. Xiang, X. Li, K. Deng, Interactive liver tumor segmentation from ct scans using support vector classification with watershed, in: Engineering in medicine and biology society, EMBC, 2011 annual international conference of the IEEE, IEEE, 2011, pp. 6005–6008.

[97] M.-P. Jolly, L. Grady, 3d general lesion segmentation in ct, in: Biomedical Imaging: From Nano to Macro, 2008. ISBI 2008. 5th IEEE International Symposium on, IEEE, 2008, pp. 796–799.

[98] Y. Qi, W. Xiong, W. K. Leow, Q. Tian, J. Zhou, J. Liu, T. Han, S. K. Venkatesh, S.-c. Wang, Semi-automatic segmentation of liver tumors from ct scans using bayesian rule-based 3d region growing, in: MICCAI workshop, Vol. 41, 2008, p. 201.

[99] D. Wong, J. Liu, Y. Fengshou, Q. Tian, W. Xiong, J. Zhou, Y. Qi, T. Han, S. Venkatesh, S.-c. Wang, A semi-automated method for liver tumor segmentation based on 2d region growing with knowledge-based constraints, in: MICCAI workshop, Vol. 41, 2008, p. 159.

[100] Y. Häme, M. Pollari, Semi-automatic liver tumor segmentation with hidden markov measure field model and non-parametric distribution estimation, Medical Image Analysis 16 (1) (2012) 140–149.

[101] 3dircadb — ircad france, <https://www.ircad.fr/research/3dircadb/>, (Accessed on 01/12/2019).

[102] B. Van Ginneken, T. Heimann, M. Styner, 3d segmentation in the clinic: A grand challenge, 3D segmentation in the clinic: a grand challenge (2007) 7–15.

[103] K. Clark, B. Vendt, K. Smith, J. Freymann, J. Kirby, P. Koppel, S. Moore, S. Phillips, D. Maffitt, M. Pringle, et al., The cancer imaging archive (tcia): maintaining and operating a public information repository, Journal of digital imaging 26 (6) (2013) 1045–1057.

[104] K. S. L. Y. B. O. K. M. G. C. . L. J. Erickson, B. J., Tcg-a-lihc - the cancer imaging archive (tcia) public access, <http://doi.org/10.7937/K9/TCIA.2016.1MMQW8UQ>, (Accessed on 01/12/2019) (2016).

[105] K. Cleary, Midas - original datasets, <http://insight-journal.org/midas/item/view/1346>, (Accessed on 01/12/2019) (2017).

[106] A. Koehn, M. C. De Dobbelaer, Bart, H. Meine, J. Meakin, M. Koek, S. Kerkstra, Grand-challenges, <https://grand-challenge.org/>.

[107] H. Kirişli, M. Schaap, C. Metz, A. Dharampal, W. B. Meijboom, S.-L. Papadopoulou, A. Dedic, K. Nieman, M. De Graaf, M. Meijs, et al., Standardized evaluation framework for evaluating coronary artery stenosis detection, stenosis quantification and lumen segmentation algorithms in computed tomography angiography, Medical image analysis 17 (8) (2013) 859–876.

[108] R. Karim, M. Varela, P. Bhagirath, R. Morgan, J. M. Behar, R. J. Housden, R. Rajani, O. Aslanidi, K. S. Rhode, Segmentation challenge on the quantification of left atrial wall thickness, in: International Workshop on Statistical Atlases and Computational Models of the Heart, Springer, 2016, pp. 193–200.

[109] O. Bernard, B. Heyde, M. Alessandrini, D. Barbosa, S. Camarasu-Pop, F. Cervenansky, S. Valette, O. C. Mirea, E. Galli, M. Geleijnse, et al., Challenge on endocardial three-dimensional ultrasound segmentation (cetus), in: Proceedings MICCAI challenge on echocardiographic three-dimensional ultrasound segmentation (CETUS), 2014, pp. 1–8.

[110] C. Petitjean, M. A. Zuluaga, W. Bai, J.-N. Dacher, D. Grosgeorge, J. Caudron, S. Ruan, I. B. Ayed, M. J. Cardoso, H.-C. Chen, et al., Right ventricle segmentation from cardiac mri: a collation study, *Medical image analysis* 19 (1) (2015) 187–202.

[111] X. Zhuang, Challenges and methodologies of fully automatic whole heart segmentation: A review, *Journal of Healthcare Engineering* (3) (2013) 371–407.

[112] G. Litjens, R. Toth, W. van de Ven, C. Hoeks, S. Kerkstra, B. van Ginneken, G. Vincent, G. Guillard, N. Birbeck, J. Zhang, et al., Evaluation of prostate segmentation algorithms for mri: the promise12 challenge, *Medical image analysis* 18 (2) (2014) 359–373.

[113] O. A. J. del Toro, O. Goksel, B. Menze, H. Müller, G. Langs, M.-A. Weber, I. Eggel, K. Gruenberg, M. Holzer, G. Kotsios-Kontokotsios, et al., Visceral–visual concept extraction challenge in radiology: Isbi 2014 challenge organization, *Proceedings of the VISCERAL Challenge at ISBI 1194* (2014) 6–15.

[114] B. Menze, A. Jakab, S. Bauer, J. Kalpathy-Cramer, K. Farahani, J. Kirby, Y. Burren, N. Porz, J. Slotboom, R. Wiest, L. Lanczi, E. Gerstner, M.-A. Weber, T. Arbel, B. Avants, N. Ayache, P. Buendia, L. Collins, N. Cordier, J. Corso, A. Criminisi, T. Das, H. Delingette, C. Demiralp, C. Durst, M. Dojat, S. Doyle, J. Festa, F. Forbes, E. Geremia, B. Glocker, P. Golland, X. Guo, A. Hamamci, K. Iftekharuddin, R. Jena, N. John, E. Konukoglu, D. Lashkari, J. Antonio Mariz, R. Meier, S. Pereira, D. Precup, S. J. Price, T. Riklin-Raviv, S. Reza, M. Ryan, L. Schwartz, H.-C. Shin, J. Shotton, C. Silva, N. Sousa, N. Subbanna, G. Szekely, T. Taylor, O. Thomas, N. Tustison, G. Unal, F. Vasseur, M. Wintermark, D. Hye Ye, L. Zhao, B. Zhao, D. Zikic, M. Prastawa, M. Reyes, K. Van Leemput, The Multimodal Brain Tumor Image Segmentation Benchmark (BRATS), *IEEE Transactions on Medical Imaging* 34 (10) (2014) 1993–2024. doi:10.1109/TMI.2014.2377694.  
URL <https://hal.inria.fr/hal-00935640>

[115] I. Işgum, M. J. Benders, B. Avants, M. J. Cardoso, S. J. Counsell, E. F. Gomez, L. Gui, P. S. Hüppi, K. J. Kersbergen, A. Makropoulos, et al., Evaluation of automatic neonatal brain segmentation algorithms: the neobrains12 challenge, *Medical image analysis* 20 (1) (2015) 135–151.

[116] G. Sanroma, O. M. Benkarim, G. Piella, K. Lekadir, N. Hahner, E. Eixarch, M. A. G. Ballester, Learning to combine complementary segmentation methods for fetal and 6-month infant brain mri segmentation, *Computerized Medical Imaging and Graphics* 69 (2018) 52–59.

[117] N. C. Codella, D. Gutman, M. E. Celebi, B. Helba, M. A. Marchetti, S. W. Dusza, A. Kalloo, K. Liopyris, N. Mishra, H. Kittler, et al., Skin lesion analysis toward melanoma detection: A challenge at the 2017 international symposium on biomedical imaging (isbi), hosted by the international skin imaging collaboration (isic), in: *Biomedical Imaging (ISBI 2018)*, 2018 IEEE 15th International Symposium on, IEEE, 2018, pp. 168–172.

[118] O. Maier, B. H. Menze, J. von der Gabeltz, L. Häni, M. P. Heinrich, M. Liebrand, S. Winzeck, A. Basit, P. Bentley, L. Chen, et al., Isles 2015-a public evaluation benchmark for ischemic stroke lesion segmentation from multispectral mri, *Medical image analysis* 35 (2017) 250–269.

[119] X. Deng, G. Du, 3d segmentation in the clinic: a grand challenge ii-liver tumor segmentation, in: *MICCAI workshop*, 2008.

[120] M. Villegas, H. Müller, A. Gilbert, L. Piras, J. Wang, K. Mikolajczyk, A. G. S. de Herrera, S. Bromuri, M. A. Amin, M. K. Mohammed, et al., General overview of imageclef at the clef 2015 labs, in: *International conference of the cross-language evaluation forum for European languages*, Springer, 2015, pp. 444–461.

[121] K. Kubota, M. Makuuchi, K. Kusaka, T. Kobayashi, K. Miki, K. Hasegawa, Y. Harihara, T. Takayama, Measurement of liver volume and hepatic functional reserve as a guide to decision-making in resectional surgery for hepatic tumors, *Hepatology* 26 (5) (1997) 1176–1181.